

## Research Article

# A Microfluidic Thyroid-Liver Platform to Assess Chemical Safety in Humans

Julia Kühnlenz<sup>1,2</sup>, Diana Karwelat<sup>3</sup>, Thomas Steger-Hartmann<sup>3</sup>, Marian Raschke<sup>3</sup>, Sophie Bauer<sup>2</sup>, Özlem Vural<sup>3,4</sup>, Uwe Marx<sup>2</sup>, Helen Tinwell<sup>1</sup> and Remi Bars<sup>1</sup>

<sup>1</sup>CropScience Division, Toxicology, Bayer S.A.S., Lyon, France; <sup>2</sup>TissUse GmbH, Berlin, Germany; <sup>3</sup>Pharmaceuticals Division, Investigational Toxicology, Bayer AG, Berlin, Germany; <sup>4</sup>Medical Biotechnology, Institute for Biotechnology, Technische Universität Berlin, Berlin, Germany

### Abstract

Thyroid hormones (THs) are crucial regulators of human metabolism and early development. During the safety assessment of plant protection products, the human relevance of chemically induced TH perturbations observed in test animals remains uncertain. European regulatory authorities request follow-up *in vitro* studies to elucidate human-relevant interferences on thyroid gland function or TH catabolism through hepatic enzyme induction. However, human *in vitro* assays based on single molecular initiating events poorly reflect the complex TH biology and related liver-thyroid axis. To address this complexity, we present human three-dimensional thyroid and liver organoids with key functions of TH metabolism. The thyroid model resembles *in vivo*-like follicular architecture and a TSH-dependent triiodothyronine synthesis over 21 days, which is inhibited by methimazole. The HepaRG-based liver model, secreting the critical TH-binding proteins albumin and thyroxine-binding globulin, emulates an active TH catabolism via the formation of glucuronidated and sulfated thyroxine (gT4/sT4). Activation of the nuclear receptors PXR and AHR was demonstrated via the induction of specific CYP isoenzymes by rifampicin, pregnenolone-16 $\alpha$ -carbonitrile, and  $\beta$ -naphthoflavone. However, this nuclear receptor activation, assumed to regulate UDP-glucuronosyltransferases and sulfotransferases, appeared to have no effect on gT4 and sT4 formation in this human-derived hepatic cell line model. Finally, established single-tissue models were successfully co-cultured in a perfused two-organ chip for 21 days. In conclusion, this model presents a first step towards a complex multimodular human platform that will help to identify both direct and indirect thyroid disruptors that are relevant from a human safety perspective.

## 1 Introduction

Thyroid hormones (THs) are fundamental for metabolic equilibrium in mammals and the growth and cognitive development of their offspring (Bassett and Williams, 2003; Bernal, 2007; Fukuchi et al., 2002; Sinha et al., 2018; Vargas-Uricoechea et al., 2014). As impairments of the hypothalamic-pituitary-thyroid (HPT) axis may cause severe adverse effects (Patel et al., 2011; Willoughby et al., 2013), the evaluation of the effects of chemicals on this axis has gained increasing importance over the last decades. In retrospect, several chemicals that have been in use for many years were identified as potential disruptors of the HPT axis (Crivellente et al., 2019; Leemans et al., 2019).

To prevent the marketing of such substances in the future and to increase the safety of novel substances, continuing effort is made by the regulatory authorities to provide scientific guidance

for the identification of endocrine disruptors. In this respect, the European Chemicals Agency (ECHA) and the European Food Safety Authority (EFSA) published a guidance document in 2018 (ECHA and EFSA et al., 2018). According to this guidance, rodent studies play a central role in the identification of endocrine disruption by plant protection products (PPP). If endocrine-related effects such as histopathologic changes of the thyroid gland are observed, with or without TH changes, mechanistic follow-up studies are required to identify the precise mode of action (MoA) in the target species (ECHA and EFSA et al., 2018). Unless proven otherwise, the MoAs identified for the rodent are also considered as being relevant for humans, which would lead to significant market restrictions for the compound under investigation. Therefore, mechanistic follow-up studies are necessary to examine if the identified MoA observed in rodents also applies to humans (ECHA and EFSA et al., 2018).

Received August 26, 2021; Accepted April 13, 2022;  
Epub May 9, 2022; © The Authors, 2023.

ALTEX 40(1), 61–82. doi:10.14573/altex.2108261

Correspondence: Julia Kühnlenz, Dr Ing.  
Bayer SAS  
16 Rue Jean-Marie Leclair  
69009 Lyon, France  
(julia.kuehnlenz1@bayer.com)

This is an Open Access article distributed under the terms of the Creative Commons Attribution 4.0 International license (<http://creativecommons.org/licenses/by/4.0/>), which permits unrestricted use, distribution and reproduction in any medium, provided the original work is appropriately cited.



Especially in the context of thyroid perturbations, concerns arose about how to determine to what extent a response in rodents reflects the response in humans (EC, 2017). In both species, the synthesis of the THs thyroxine (T4) and the biologically active form 3,3',5-triiodothyronine (T3) are controlled by a complex feedback mechanism within the HPT axis (Abel et al., 2001; Dumont, 1971; Nikrodhanond et al., 2006). In addition, the liver contributes to a balanced TH homeostasis by metabolizing THs either by deiodination, mainly via the type 1 deiodinase (DIO1), or by inactivation via the phase II enzymes uridine diphosphate glucuronosyltransferases (UGTs) and sulfotransferases (SULTs) (van der Spek et al., 2017). These enzymes transform T3 and T4 into their glucuronide and sulfate conjugates (gT4 and sT4, gT3 and sT3), which are excreted via the bile (van der Spek et al., 2017).

Even though these mechanisms apply to both rodents and humans, there is evidence that rodents have an increased sensitivity to impairments in TH homeostasis. Humans have a slower TH turnover, with increased half-lives of T4 and T3. Most notably, there are marked species differences in TH binding affinities to the TH carrier proteins (albumin, TH-binding globulin (TBG), and transthyretin (TTR)) (Bartsch et al., 2018; Foster et al., 2021; Meek et al., 2003). The liver-secreted carrier proteins present one main storage site of the THs and bind up to 99.5% of the THs found in human blood serum (EC, 2017). TBG, being with 20 mg/L blood serum much less abundant than albumin (45 mg/L blood serum), contributes the most (75%) to the total bound T3 and T4 fraction and thus is crucial for the maintenance of TH levels (EC, 2017; Hotari et al., 1987; Hammond et al., 2019). Variations in TH carrier protein concentrations, in particular TBG, are associated with changes in total TH serum levels without strikingly altering the euthyroid state (Bartalena and Robbins, 1992; Domingues et al., 2009). Furthermore, altered TH levels are associated with interactions between TH carrier proteins and xenobiotics, resulting in TH displacement (Hallgren and Darnarud, 2002; Marchesini et al., 2008). As a consequence, abnormalities in TH carrier protein levels or chemical-induced TH replacements are considered putative molecular initiating events (MIE) leading to TH-related neurodevelopmental toxicity (AOP 152) (Noyes et al., 2019). To our knowledge, few human hepatic *in vitro* models have been characterized with regard to their TBG and TTR secretion ability, meaning their capability to investigate related adverse outcome pathways (AOP) is unknown. In addition to the differential TH binding capacities between humans and rodents, differences in the TH catabolism pathways are apparent, with rodents showing a more active hepatic TH degradation via the UGT enzymes (Bartsch et al., 2018; Richardson et al., 2014).

As mentioned above, the mechanisms of TH perturbation were

recently summarized in an AOP network, where a total of 26 MIEs that may be implicated in thyroid hormone disruption and subsequent downstream adverse effects are listed (Noyes et al., 2019). Several *in vitro* high-throughput assays exist that investigate the main MIEs for chemically induced thyroid activity. They either involve the thyroid gland directly (direct thyroid toxicity) or target TH catabolism through the induction of hepatic enzymes (indirect thyroid toxicity) (Noyes et al., 2019). While these assays are useful for early-stage development of new compounds, they are limited to the evaluation of molecular and biochemical interactions between cellular targets and the compound of interest while neglecting the physiological environment and functionality of target tissue. To better assess whether the identified MoA in rodents also applies to humans, new *in vitro* test methods with human cells or tissues that more accurately emulate TH homeostasis are needed to directly evaluate the physiological effect of xenobiotics. Microphysiological systems with their properties of flow-through and integration of different tissue models have the potential to improve such an *in vitro* assessment. We therefore investigated a novel two-organ combination of human thyroid and liver organoids that simulates both TH biosynthesis and hepatic TH catabolism.

TH biosynthesis in the thyroid gland is one of the main target sites of xenobiotics (DeVito et al., 1999). Given the structure-function relation of thyroid follicles, which are the smallest functional subunit of the thyroid gland, the follicular arrangement and correct cell polarization of thyrocytes is key to model TH synthesis *in vitro*. Whereas thyroglobulin (TG) (the precursor molecule of the THs) is enriched in the interior of the follicles (the colloid), cell pole specifically expressed transport proteins generate an intrafollicular reservoir of iodine (Goodman, 2009). During TH synthesis, iodine is oxidized and coupled to the tyrosine residues of TG, forming the TH precursors of T3 and T4 (Mondal et al., 2016). To preserve the native cell polarity and maintain thyroid-specific functionalities, extracellular matrix (ECM)-based three-dimensional (3D) thyrocyte cultures are required to remodel intrafollicular enrichment of iodine and TG, iodination of TG, thyroid-stimulating hormone (TSH) responsiveness, and TH secretion (Chambard et al., 1981; Deisenroth et al., 2020; Garbi et al., 1986; Kraiem et al., 1991; Kusunoki et al., 2001; Massart et al., 1988; Nishida et al., 1993; Saito et al., 2018; Sasaki et al., 1991; Toda et al., 1992, 2011). Besides one recently published 3D thyroid model generated from primary human thyrocytes (Deisenroth et al., 2020), no other standardized models currently exist to study thyroid-relevant MoAs in humans in a physiologically relevant manner. For this reason, we developed an *in vitro* thyroid model that emulates TH biosynthesis and its chemically induced impairment leading to changes in TH secretion.

#### Abbreviations

2D, two-dimensional; 3D, three-dimensional; AHR, aryl hydrocarbon receptor; AOP, adverse outcome pathway; ATP, adenosine triphosphate; BNF,  $\beta$ -naphthoflavone; cAMP, cyclic adenosine monophosphate; CYP, cytochrome P450; DIO1, type 1 deiodinase; ECHA, European Chemicals Agency; ECM, extracellular matrix; EFSA, European Food Safety Authority; FBS, fetal bovine serum; GFR, growth factor-reduced; gT4, T4 glucuronide; HPT, hypothalamic-pituitary-thyroid; HStEC, human hepatic stellate cells; MCT8, monocarboxylate transporter 8; MIE, molecular initiating event; MMI, methimazole; MoA, mode of action; MOC, multi-organ chip; MRP2, multidrug resistance-associated protein 2; NAM, new approach methodology; PCN, pregnenolone-16 $\alpha$ -carbonitrile; PHH, primary human hepatocytes; PPP, plant protection products; PS, penicillin-streptomycin; PXR, pregnane X receptor; RIF, rifampicin; RT, room temperature; sT4, T4 sulfate; SULT, sulfotransferase; T3, 3,3',5-triiodothyronine; T4, thyroxine; T4-UGT, UGT activity for T4; TBG, thyroxine-binding protein; TG, thyroglobulin; TH, thyroid hormone; TSH, thyroid-stimulating hormone; TTR, transthyretin; UGT, uridine diphosphate glucuronosyltransferase; ULA, ultra-low attachment; ZO1, tight junction protein-1

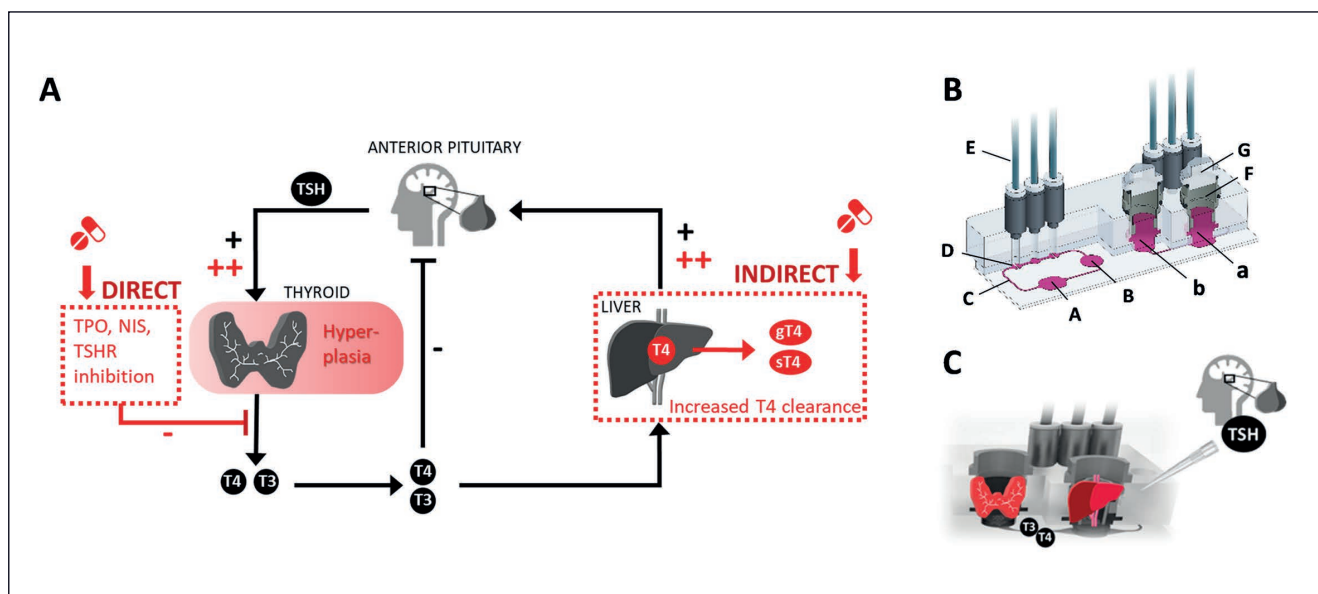


**Fig. 1: Hepatic-thyroid axis and its implementation *in vitro***

(A) Feedback mechanism of thyroid hormone synthesis through the liver and anterior pituitary gland and its chemically induced disruption. Black elements represent the native state whereas red ones indicate the perturbation. gT4, glucuronidated T4; NIS, sodium/iodide symporter; sT4, sulfated T4; T3, triiodothyronine; T4, thyroxine; TPO, thyroid peroxidase; TSH, thyroid-stimulating hormone; TSHR, TSH receptor. (B) Presentation of a 2-organ-chip containing two identical culture circulations. Left circulation presents a plan view showing the bottom areas of the outer [A] and inner [B] culture compartment, which are interconnected by microchannels [C]. Three pump membranes integrated in the channel system [D], which are moved up and down by microtube [E]-delivered pressure/vacuum, enable the medium perfusion of the culture system. The right circulation shows the cross-sectional view of the outer [a] and inner [b] culture compartment including in pink the level of the culture medium, the screwed-in culture inserts and lids. (C) Schematic representation of the *in vitro* simulated hepatic-thyroid axis and the systemic application of TSH representing the pituitary. Depicted is a cross-section of one circulation of the 2-organ-chip platform showing thyroid and liver models in separate culture compartments.

Besides TH biosynthesis, a number of xenobiotics indirectly affect the thyroid gland by targeting hepatic TH catabolism via activation of xenobiotic nuclear receptors and thus associated induced UGT activity for T4 (T4-UGT) in rodents (Hood et al., 2003; Meek et al., 2003; Rouquié et al., 2014). According to recent data collections, 60 out of 128 small molecules tested were considered to provoke TH perturbations via liver enzyme inductions (Crivellente et al., 2019). However, little is known about the correlation between increased T4-UGT activity and thyroid adverse effects in humans. In this context, new human-relevant *in vitro* assays are required that not only study hepatic nuclear receptor activations as putative MIEs but directly evaluate changes in gT4 and sT4 catabolite formation. Apart from a two-dimensional (2D) human sandwich-cultured hepatocyte model (Richardson et al., 2014), to our knowledge there are limited published assays addressing this in detail. In recent years, major efforts in 3D culture techniques have been directed towards the formation of 3D liver spheroids whose cell-cell interactions and native metabolic zonation reinforce the hepatic phenotype while increasing liver-like functionality compared to 2D monolayers (Cox et al., 2020; Langan et al., 2016; Lauschke et al., 2016; Underhill and Khetani, 2018). Overcoming the limited life-span of hepatic 2D cultures, the 3D structure prevents the dedifferentiation of he-

patocytes and thus allows long-term culture up to 5 weeks with maintained hepatocyte-specific functions (Bell et al., 2016; Elaut et al., 2006; Gunness et al., 2013; Kanebratt et al., 2021; Leite et al., 2012; Mandon et al., 2019; Ramaiahgari et al., 2017; Zellmer et al., 2010).

Here, we extensively characterize a 3D liver spheroid model composed of the HepaRG™ cell line and structure-supporting human hepatic stellate cells (HStc) (Abu-Absi et al., 2004). Based on several reports, the HepaRG cell line is considered an appropriate alternative to primary human hepatocytes (PHH) with good morphologic and metabolic similarities (Aninat et al., 2006; Hoekstra et al., 2013; Huaman et al., 2012; Kammerer and Küpper, 2018; Lübberstedt et al., 2011; Tascher et al., 2019) and a high relevance to assess drug safety (Hendriks et al., 2016; Li et al., 2019; Tomida et al., 2015; Wang, Z.-Y. et al., 2019). Furthermore, there is evidence that HepaRG cells are able to produce glucuronidated and sulfated metabolites *in vitro* (Darnell et al., 2012; Richter et al., 2016; Yokoyama et al., 2018), making these cells suitable to study TH catabolite formation. As demonstrated in this study, the HepaRG/HStc liver spheroid model was capable of reproducing TH catabolism by synthesizing gT4 and sT4.

Given the complexity of TH homeostasis, which is affected by both direct and indirect impairment of the thyroid gland (Fig. 1),



the final aim of the study was the functional co-cultivation of the pre-characterized thyroid and liver organ models in a commercially available multi-organ chip (MOC) platform produced under ISO 9001-2015 standards.

## 2 Materials and methods

Cell cultures were handled under a sterile safety cabinet and according to the guidance on Good Cell Culture Practice (Coecke et al., 2005). Their maintenance took place at 37°C and 5% CO<sub>2</sub> in a humidified incubator. Animal-derived components such as FBS, Matrigel or TSH are subject to replacement by animal-free alternatives once these are readily available and fully validated.

### Cell culture medium formulations

Storage medium for freshly dissected thyroid tissue consisted of William's E medium (PAN Biotech) supplemented with 0.25 µg/mL amphotericin (Corning) and 5 µg/mL gentamycin (Corning). HStcC were pre-cultured in optimized medium from ScienCell (SC basal medium, 1% SC supplements, 2% FBS, 1% penicillin-streptomycin (PS)). Prior to spheroid formation, HepaRG™ cells were maintained in William's E medium w/o L-glutamine w/o phenol red, 10% fetal bovine serum (FBS, Provitro AG), 2 mM L-glutamine, 50 µM hydrocortisone 21-hemisuccinate sodium salt (VWR), 5 mg/L insulin (PAN Biotech), 5 µg/mL gentamycin, 250 ng/mL amphotericin, and 2% DMSO to avoid dedifferentiation of the cells. Spheroid formation of HepaRG cells and HStcC took place in William's E medium w/o L-glutamine w/o phenol red, 10% FBS, 2 mM L-glutamine, 50 µM hydrocortisone 21-hemisuccinate sodium salt, 5 mg/L insulin, 5 µg/mL gentamycin, 250 ng/mL amphotericin, and 10% FBS. The co-culture medium used for thyroid and liver single organ cultures and the optimized co-culture approach is based on the chemically defined, serum-free SILAC Advanced DMEM/F-12 Flex no glucose/no phenol red medium (Thermo Fisher) with 2 mM L-glutamine (Corning), 0.1 µM sodium iodine (SIGMA), 1% MEM amino acids - 50x solution [-] L-glutamine (Corning), 0.1 µM dexamethasone (SIGMA), 5 µg/mL gentamycin, and 250 ng/mL amphotericin.

### Thyroid model generation

The procedure is visualized in Figure S1<sup>1</sup>. Human thyroid tissue was obtained with informed consent from patients with unknown health state but negatively tested for human immunodeficiency virus (HIV), hepatitis B virus (HBV) and hepatitis C virus (HCV). Donor gender, age, and smoker status are given in Table 1. After removal of the thyroid explant, the tissue was collected in its storage medium and kept at 4°C. Follicle isolation was performed within 12 h.

The thyroid explant was washed 2 × with PBS (Corning), rinsed with 80% ethanol (VWR), and rehydrated in PBS. Non-pathological tissue was chopped with a curved scissor and transferred into a 10 mL collagenase/dispase II solution (2 mg/mL

**Tab. 1: Specifications of the 13 thyroid donors of the study**

Thyroid donor	Gender	Age	Smoker
1	unknown	46	no
2	female	47	no
3	female	53	yes
4	female	79	no
5	female	62	no
6	female	45	yes
7	female	50	unknown
8	female	46	unknown
9	female	79	no
10	male	56	unknown
11	male	50	unknown
12	female	31	no
13	female	53	no

collagenase NB 4 (Nordmark) and 4 mg/mL Dispase II (SIGMA) diluted in William's E medium containing 5 µg/mL gentamycin). Thyroid tissue was digested for 3 h under constant rotation. Every hour the already isolated thyroid follicles were harvested from the supernatant, and sedimented, undigested tissue was covered in fresh collagenase/dispase II solution. Supernatant was filtered through a 100 µm cell strainer, which was rinsed with 20 mL PBS, and centrifuged for 10 min at 30 g. The follicle pellet was resuspended in 1 mL co-culture medium + 10% FBS with a 1 mL wide bore pipet tip to avoid shear stress. Resuspended follicles were transferred into a T75 ultra-low attachment (ULA) flask (Corning) containing 12 mL co-culture medium supplemented with 10% FBS. The latter was required to minimize aggregate formation and attachment between freshly isolated follicles, which were recovered overnight in suspension culture. The following day, follicles were centrifuged in a 50 mL falcon for 10 min at 30 g. Erythrocytes were removed by 20 min lysis in erythrocyte lysis buffer (PAN Biotech) at room temperature (RT). The process was stopped by adding co-culture medium + 10% FBS. Pelleted follicles (5 min, 30 g) were resuspended and 50 µL counted in a 96-well plate (Corning) (n = 5) neglecting small follicle fragments. In case of aggregates, the apparent number of follicles per aggregate was counted. 1000 follicles were embedded in 50 µL growth factor-reduced (GFR) Matrigel (Corning) using 1.5 mL tubes. After 1 h polymerization at 37°C, 100 µL co-culture medium was added. The next day, matrix-follicle drops were transferred with a curved spatula into either a 48-well plate (static) or the inner culture compartment of the Chip2 device, see below, containing 400 µL or 200 µL co-culture medium, respectively. In order to generate the thyroid models for subsequent intracellular measurements of adenosine

<sup>1</sup> doi:10.14573/altex.2108261s

triphosphate (ATP) or cAMP, 20  $\mu$ L of the previously described GFR Matrigel follicle solution containing approximately 300 follicles was transferred into a flat-bottom 96-well ULA plate. After 1 h polymerization at 37°C, 160  $\mu$ L co-culture medium was added to each well.

#### *HUMIMIC Chip2*

The microphysiological organ-chip (HUMIMIC Chip2) was designed and fabricated at TissUse GmbH. It is composed of two culture compartments, which are interconnected by a microfluidic channel system of 100  $\mu$ m height. An on-chip micro-pump generates a pulsatile flow of the systemic culture medium, enabling cross-talk between the organ models. Within the here presented scope, the following settings were applied: pressure 300 mbar, vacuum -300 mbar, pump frequency 0.45 Hz, direction of flow (left circuit) clockwise, direction of flow (right circuit) anti-clockwise. Prior to organoid culture, cell-free Chip2s were pre-incubated with co-culture medium for 2 days to saturate the surface.

#### *Thyroid single culture*

Thyroid follicle models, cultured either in 48-well plates or in the inner compartment of the Chip2, were maintained for up to 29 days. Culture supernatants were completely removed every 2 to 3 days and replaced with 400  $\mu$ L co-culture medium freshly supplemented with 0.1, 1 or 10 mIU/mL TSH (thyroid-stimulating hormone, bovine pituitary, Creative Biomart). For the chip-based culture, 200  $\mu$ L medium was added per culture compartment. Collected supernatants were analyzed for TH secretion by LC-MS/MS analysis. Difference in overall T3 secretion between 0.1 and 1 mIU/mL TSH treatment groups was evaluated by an unpaired t-test of log-transformed T3 concentrations over the whole time. Each group contained three intra-donor replicates. At the end of culture, thyroid follicle models were fixed for immunostaining.

#### *Cyclic adenosine monophosphate (cAMP) measurement*

96-well plate-based thyroid follicle cultures from three or two independent donors divided in seven TSH exposure groups (0 (n = 3), 0.1 (n = 3), 1 (n = 3), 5 (n = 2), 10 (n = 3), 50 (n = 2) and 100 (n = 2) mIU/mL, which each included technical intra-donor triplicates), were initially cultured for 7 days without TSH. On day of cAMP analysis, thyroid follicles were treated with the respective TSH concentration or 10  $\mu$ M forskolin (positive control, (n = 3), Cayman Chemical Company) diluted in co-culture medium containing 500  $\mu$ M 3-isobutyl-1-methylxanthine (IBMX, SIGMA) and 100  $\mu$ M imidazolidinone (SIGMA), both inhibitors of cAMP hydrolysis, for 1 h (160  $\mu$ L/well). Intracellular cAMP content was measured by cAMP-Glo™ Assay (Promega): cell lysis was induced by replacing the culture medium with 20  $\mu$ L lysis buffer and constant orbital agitation (700 rpm) for 30 min at RT. Lysate was thoroughly mixed with 40  $\mu$ L cAMP Glo-detection reagent by orbital shaking at 700 rpm for 1 min and incubated at RT for an additional 20 min. 80  $\mu$ L kinase-Glo reagent was added, thoroughly mixed, and 120  $\mu$ L were transferred to a clear-bottom white polystyrene microplate. Luminescence was measured immediately. Blank-corrected raw data were log-transformed to achieve Gaussian distribution according

to the Shapiro-Wilk test. Statistical analysis between TSH-treated and non-treated conditions was performed by one-way ANOVA using Dunnett's post hoc test and intradonor matching for 0.1/1/10 mIU/mL TSH and forskolin-treated models as three independent donors were tested here. Geisser-Greenhouse correction was included into statistical analysis as no equal variance between test conditions existed. The treatment groups 5/50/100 mIU/mL TSH were not statistically analyzed as data from only two independent human donors were collected.

#### *Methimazole (MMI) treatment*

Thyroid follicle models of 4 independent human donors containing two or three intradonor replicates were pre-cultured with 1 mIU/mL TSH for 3 days in 48-well plates. MMI (SIGMA), a reference thyroid peroxidase (TPO)-inhibitor, was dissolved in DMSO (VWR) and subsequently in co-culture medium to a final DMSO concentration of 0.1% in a step-wise dilution series of 10, 1, 0.1 and 0  $\mu$ M MMI. Thyroid models were each treated with 400  $\mu$ L of the respective MMI dilution for 2 days. Subsequently the MMI-dosing was renewed for an additional 2 days to achieve a 4-day treatment in total. Collected culture supernatants were analyzed by LC-MS/MS analysis for T3 formation. T3 concentrations of each donor and condition were normalized (%) to mean T3 concentration of DMSO on the same day. To determine toxicity of MMI doses, the total intracellular ATP content was simultaneously assessed via the CellTiter-Glo 3D cell viability assay (Promega) in thyroid follicles cultured in 96-well plates and treated for 7 days with 0/0.1/1/10  $\mu$ M MMI. For data analysis, blank-corrected measurement values were log-transformed to achieve Gaussian distribution according to Shapiro-Wilk test and assure homogeneity of variance as tested by Brown-Forsythe test. Differences between these data sets were evaluated by one-way ANOVA using Dunnett's multiple comparison and data matching within single donors.

#### *Liver model generation*

The liver model is derived from the HepaRG cell line, a hepatoma human cell line with the potential to differentiate into both biliary-like and hepatocyte-like cells. Cryopreserved differentiated HepaRG cells (Biopredic, HPR116080, passage 0, negative tested for mycoplasma and microbial growth), seeded at a density of  $0.2 \times 10^6$  cells/cm<sup>2</sup>, were pre-cultured for 4 days in HepaRG maintenance culture medium. Cryopreserved HStcC (ScienCell, 5300, Lot: 16646, negative tested for HIV-1, HBV, HCV, mycoplasma, bacteria, yeast and fungi) at passages between 2 and 4 were pre-cultured for 3 days at confluence below 80% in HStcC culture medium. HepaRG cells were harvested using 0.25% trypsin/2.21 mM ethylenediaminetetraacetic acid (EDTA) (Corning). HStcC were harvested with 0.05% trypsin/0.53 mM EDTA (Corning).  $1 \times 10^4$  HepaRG cells and 400 HStcC were seeded per well of a 384-well ULA spheroid plate (Corning) in spheroid formation medium. Plates were centrifuged for 1 min at 300 g. Liver spheroids formed after 4 days. 25 liver spheroids were transferred from a 384-ULA plate into flat-bottom 96-well ULA plates (Corning) using an electronic 15-300  $\mu$ L pipette in multi-aspirate mode (20  $\mu$ L/step) with 200  $\mu$ L wide-bore filter tips. Medium-freed liv-



er spheroids then were embedded in 50  $\mu\text{L}$  2 mg/mL collagen I (R&D systems). Even distribution of the 25 liver spheroids per collagen I gel was ensured by immediately circling the plate by hand. After 30 min polymerization of the collagen I matrix at 37°C, 100  $\mu\text{L}$  co-culture medium was added to each liver spheroid-gel. Next day, two liver spheroid gels (HepaRG/HStECs liver spheroid model) were transferred into either a 48-well plate or the outer culture compartment of the Chip2 containing 400  $\mu\text{L}$  or 200  $\mu\text{L}$  co-culture medium, respectively. Liver model generation is illustrated in Figure S2<sup>1</sup>.

#### *Liver single culture*

Day 0 controls for RNA isolation and immunostaining were immediately taken after the liver spheroids were picked and prior to collagen I embedding. Samples were stored at -80°C and 4°C, respectively, until further processing. Liver spheroids, cultured either in 48-well plates or the outer compartment of the Chip2, were maintained in co-culture medium for 14 to 21 days. Medium was completely exchanged every 2 to 3 days while the albumin and TBG concentrations in the collected supernatants were assessed via the Albumin in Urine/CSF FS kit according to the manufacturer's instructions (Diagnostic Systems, 10242) and the Human Serpin A7 PicoKine™ ELISA Kit (Antikörper Online, ABIN5510681), respectively. To obtain the total albumin or TBG yield per day, the albumin/TBG content ( $\mu\text{g}$ ) in 400  $\mu\text{L}$  was calculated and divided by the number of days between the medium exchanges. RNA was isolated from liver spheroids after 14-day dynamic cultivation. Optimal conditions for gT4/sT4 formation were determined in 48-well plates by exposing the HepaRG/HStECs liver spheroid model to 0.005  $\mu\text{M}$ , 0.1  $\mu\text{M}$  or 1  $\mu\text{M}$  T4 for 24 h or to 1  $\mu\text{M}$  TSH for 4 h, 16 h and 24 h on culture day 9. The gT4/sT4 concentrations were measured within the culture supernatants after the respective T4 exposure times. To evaluate a maintained TH catabolite formation under dynamic conditions, HepaRG/HStEC liver spheroids were cultured for 11 days in the Chip2. On day 11, 1  $\mu\text{M}$  T4 was freshly spiked during the medium exchange. Post 72 h., i.e., on culture day 14, the collected supernatants, temporarily stored at -20°C, were analyzed in terms of gT4/sT4 formation by LC-MS/MS analysis.

#### *Induction of phase I and II liver enzymes*

Liver spheroid models were pre-cultured in 400  $\mu\text{L}$  co-culture medium in 48-well plates for 5 days, including one medium exchange on day 2, until medium was replaced by co-culture medium supplemented with 1 or 10  $\mu\text{M}$  T4 (SIGMA) and 10  $\mu\text{M}$   $\beta$ -naphthoflavone (BNF, an aryl hydrocarbon receptor (AHR) agonist (SIGMA)) or 10  $\mu\text{M}$  rifampicin (RIF, a human-specific pregnane X receptor (PXR) agonist (SIGMA)) or 10  $\mu\text{M}$  pregnenolone-16 $\alpha$ -carbonitrile (PCN, a rodent-specific PXR agonist, (SIGMA)). A 0.1% DMSO solvent control was carried out in parallel. Induction medium was renewed after 3 days and remained until day 6. As depicted in Figure 5A, gT4 and sT4 metabolites (and albumin) were measured in culture supernatants at both time points (3 and 6 days) to broaden the time window in which putative changes in metabolite formation levels might occur. After the 6-day treatment, one liver spheroid-gel of each condition was

taken for RNA recovery whereas the other gel underwent a cytochrome P450 (CYP) induction assay. RIF and PCN-treated liver spheroids were analyzed for CYP3A4 activity by P450-Glo™ CYP3A4 Assay Kit (Promega, V9002), and CYP1A2 activity was measured in BNF-treated liver spheroids via P450-Glo™ Assay Kit (Promega, V8422) according to the manufacturer's instruction. In both assays, the time for the CYP substrate conversion was increased to 24 h, and the assay volume was set to 100  $\mu\text{L}$ . DMSO-treated liver spheroids served as reference.

#### *Co-culture*

Three co-cultures were performed with follicles from three independent human thyroid donors using 1000 thyroid follicles per condition and the HepaRG/HStEC liver spheroid model (2  $\times$  25 liver spheroids embedded in collagen I). Culture was performed over 21 days according to Figure 6. Three different conditions were executed, with triplicates each, per co-culture run: co-culture medium (1) without TSH, (2) with 0.1, and with (3) 1 mIU/mL TSH. Medium was exchanged every 2 to 3 days and, if required, freshly supplemented with TSH. During the medium exchange, 200  $\mu\text{L}$  conditioned medium was removed from each compartment and replaced with 200  $\mu\text{L}$  fresh medium to restore a total volume of approximately 400  $\mu\text{L}$ . The collected medium was combined and analyzed for TBG and albumin secretion and the formation of T4 and T3 metabolites. The morphology of the organ models was assessed at the beginning and end of culture by bright field microscopy. After 21 days of culture, thyroid follicles were recovered for immunostaining. The collagen gels of the liver model were used for RNA isolation and immunostaining.

#### *Gene expression analysis*

Liver spheroids were extracted from collagen I matrix by 25 mg/mL collagenase NB4 solution for 40 min at 37°C. Total RNA was extracted using NucleoSpin RNA Plus XS Kit (Machery-Nagel). RNA was reverse transcribed into cDNA using the TaqMan Reverse Transcription Kit (Applied Biosystems). qPCR analysis was performed with QuantStudio 5 Real-Time PCR System using a SensiFAST SYBR Lo-ROX Kit (Bioline) or TaqMan Kit (Thermo Fisher Scientific). Primers can be found in Table S1 and S2<sup>1</sup> respectively. Fold changes were calculated by comparative Ct method ( $\Delta\Delta\text{Ct}$ ). Selected housekeepers were succinate dehydrogenase complex flavoprotein subunit A SDHA (liver model) and glyceraldehyde 3-phosphate dehydrogenase (GAPDH) (thyroid model), which were validated to be not affected by experimental conditions.

#### *Histology*

Thyroid tissue was fixed with 4% formaldehyde + 0.1% glutaraldehyde for 20 min at 4°C. The liver model was fixed with 4% formaldehyde for 40 min at 4°C. Three washes with PBS followed. Samples for cryosectioning were dehydrated in aquatic sucrose solution (15% at 4°C overnight, 30% at RT for 4 h) and frozen in TissueTek. 8  $\mu\text{m}$  thyroid cryosections were stained with hematoxylin and eosin (H&E) according to standard protocols using the Tissue Stainer TST44C. For 2D immunofluorescence staining, liver model cryosections were fixed in acetone (-20°C, 10 min), washed

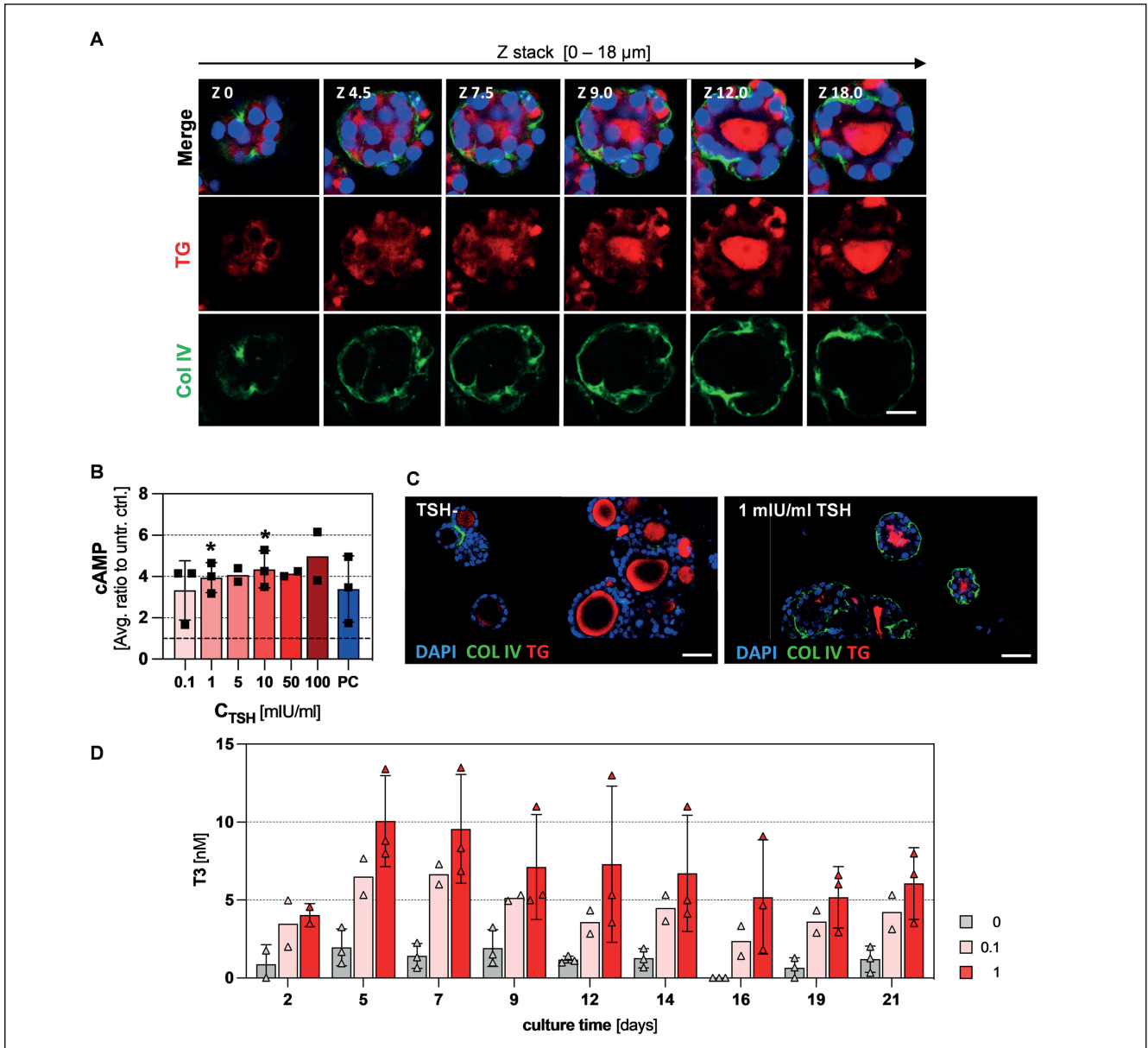


**Fig. 2: Functional characterization of the statically cultured 3D thyroid model**

(A) Confocal Z-stack image series of 29-day static cultured thyroid follicles stimulated with 1 mIU/mL TSH (Donor 1) for the duration of the culture. Intrafollicular colloid was visualized by immunofluorescent staining of thyroglobulin (TG, red, DyLight 594). Basement membrane was visualized by immunofluorescent staining of collagen IV (Col IV, green, DyLight 488). Blue corresponds to DAPI labelling the nuclei. Scale 15  $\mu$ m. (B) Intracellular cAMP content of 7-day cultured and TSH-treated thyroid follicles relative to non-treated control. 10  $\mu$ M forskolin treatment was used as a positive control (PC). Bars represent the mean ratio to TSH non-treated control of at least two independent thyroid donors ( $n \geq 2$ ) (Donor 2, 3, 4). SD is shown for  $n = 3$ . Mean of one donor, calculated from intraexperimental triplicates, is indicated by a single triangle. Differences of samples with  $n = 3$  were compared based on log-transformed raw data by one-way ANOVA with Geisser-Greenhouse correction using Dunnett's post-hoc test. Changes to control (0 mIU/mL TSH) were considered significant for  $p < 0.05$  (\*,  $p < 0.05$ ). (C) Representative immunofluorescent staining of the unstimulated (TSH-) and TSH-stimulated (1 mIU/mL TSH) 3D thyroid model after being statically cultured for 21 days. Protein expression of thyroglobulin (TG, red), collagen IV (COL IV, green), and nuclei (DAPI, blue) is shown. Scale 30  $\mu$ m. (D) TSH-dependent T3 secretion of 21-day statically cultured 3D thyroid models (Donor 5). Triiodothyronine (T3) was measured in culture supernatants from the 3D thyroid model exposed to 0 (grey), 0.1 (light red) or 1 (red) mIU/mL TSH by LC-MS/MS analysis. Bars represent the mean  $\pm$  SD of three independent thyroid donors for 0 and 1 mIU/mL TSH ( $n = 3$ ; Donor 6,7,8) or the mean of two independent thyroid donors in case of 0.1 mIU/mL TSH treatment ( $n = 2$ ; Donor 7,8) (Each triangle represents mean of an intraexperimental triplicate of one donor). Data points on the x-axis indicate T3 concentrations below limit of quantification ( $< 0.5$  nM).



twice in PBS with calcium/magnesium and treated with primary antibodies dissolved in 10% goat serum overnight at 4°C: rabbit anti-MCT8 (monocarboxylate transporter 8, Novus Biologicals, polyclonal, NBP1-89196, dilution 1:100), mouse anti-MRP2 (multidrug resistance-associated protein 2, Enzo Life Science, ALX-801-016, dilution 1:50), rabbit anti-ZO1 (tight junction protein-1, Proteintech, polyclonal, 21773-1-AP, dilution 1:100), and mouse anti-albumin (Sigma, monoclonal, A6684, dilution 1:100). After three wash steps with PBS, cryosections were incubated with secondary antibodies diluted in PBS containing 1 µg/mL DAPI for 45 min: goat anti-mouse IgG, DyLight 488 (Thermo, polyclonal, 35511, dilution 1:200) and/or goat anti-rabbit IgG, DyLight 594 (Thermo, polyclonal, 35553, dilution 1:200). After washing and mounting, images were acquired using an inverted fluorescence microscope (Keyence) and staining was normalized to respective negative control. For whole tissue 3D staining, fixed organ models were permeabilized with 0.3% Triton X-100 for 2 h at RT, washed three times with wash buffer (PBS with 0.0001% Triton X-100), and blocked with 3% goat serum + 0.1% Triton X-100 for 60 min at RT under constant agitation. Primary antibodies, diluted in 1% goat serum + 0.1% Triton X-100, were incubated at 4°C overnight: rabbit anti-MCT8, mouse anti-MRP2, rabbit anti-ZO1, mouse anti-collagen IV (Sigma, monoclonal, C1926, dilution 1:100), and rabbit anti-thyroglobulin (Abcam, monoclonal, ab156008, dilution 1:100). Secondary antibodies, previously mentioned, were diluted in wash buffer containing 1 µg/mL DAPI (Roche Diagnostics) and applied overnight at 4°C followed by three PBS washes. 15 min prior to microscopy, the samples were cleared in Visikol Histo-M (Visikol). Images were acquired with the Leica SPE8 confocal microscope.

#### LC-MS/MS analysis

T3, T4, gT4 and sT4 analytes were measured according to the method described in Karwelat et al. (2022).

#### Data analysis/statistics

Statistical analyses and data visualization were performed with Prism 7.03 software (GraphPad). Statistical analysis was only performed if data from at least three independent replicates ( $n \geq 3$ ) were present. The mentioning of  $n$  always refers to an independent experiment. Selected statistical tests are indicated in the respective material section and/or figure legend. P values are given at a 95% confidence interval and were considered significant for  $p < 0.05$  (\*,  $p < 0.05$ , \*\*,  $p < 0.01$ , \*\*\*,  $p < 0.001$ , \*\*\*\*,  $p < 0.0001$ ).

## 3 Results

### 3.1 Characterization of the *in vitro* 3D thyroid model

#### 3.1.1 Model generation and morphologic characterization

The follicular arrangement of thyrocytes and correct cellular polarization is a fundamental requirement to obtain a functional *in vitro* thyroid model (Deisenroth et al., 2020; Mauchamp et al.,

1998). To provide mechanical and structural support, isolated thyroid follicles were embedded in GFR Matrigel. The follicular organization of the cells surrounding a luminal compartment could be demonstrated after a 29-day plate-based culture. Confocal laser scanning microscopy along the z-axis clearly showed their spherical structure and indicated the maintenance of native cell polarization (Fig. 2A). The ECM component collagen IV marked the basal cell pole while enclosing the entire follicle. In addition, the TH precursor molecule TG was visualized in the luminal compartment, suggesting an intrafollicular colloid and thus a suitable reaction space for TH biosynthesis.

#### 3.1.2 Accumulation of cAMP

Given the structural similarity to the thyroid gland, we aimed to characterize the functional response of the thyroid model towards TSH, the key regulator of the thyroid gland. Upon binding to the TSH receptor localized in the basal membrane, TSH initiates a cAMP-dependent signaling cascade stimulating multiple processes required for TH biosynthesis (Dumont, 1971). Thyroid model cultures exposed to different TSH concentrations showed elevated cAMP levels being significantly increased after exposure to 1 and 10 mIU/mL TSH (Fig. 2B). A TSH concentration of 1 mIU/mL or more induced the maximal response in cAMP levels for all donors tested. This shows that the established 3D thyroid model is responsive to an external TSH-stimulus.

#### 3.1.3 TSH-dependent morphologic change

As known from *in vivo* conditions, the appearance of thyroid follicles changes with their activity state, which allows distinction between hypothyroid, euthyroid and hyperplastic states (Yuri et al., 2018, p. 6). To evaluate the stimulation of active and resting follicles *in vitro*, the 3D thyroid model was cultured in the presence or absence of 1 mIU/mL TSH for 21 days. The endpoint morphology of the follicles was visualized by immunofluorescence labeling of collagen IV and TG (Fig. 2C). Non-stimulated follicles exhibited flat, squamous-like cell nuclei with weakly stained extracellular collagen IV matrix. In comparison, TSH-stimulated cells appeared taller, with rounder nuclei, while collagen IV surrounded the whole follicle. Furthermore, distinctive differences in the colloid's shape could be detected by TG staining. Whereas non-stimulated follicles had a circular defined intrafollicular lumen, the TSH-stimulated follicles showed colloids with more uneven borders. Overall, TSH-dependent morphologic changes in the 3D thyroid model appear to be similar to those observed *in vivo*.

#### 3.1.4 Thyroid hormone secretion

To complete the functional characterization, static 3D thyroid models cultured in the absence or presence of 0.1 or 1 mIU/mL TSH were examined for secretion of T4 and T3. Unexpectedly, the 3D thyroid model hardly secreted any T4 under all conditions tested (Tab. S3<sup>1</sup>). However, in the TSH-treated groups, reproducibly stable levels of T3 were maintained between day 5 and day 21 exhibiting means of  $4.6 \pm 1.3$  nM (0.1 mIU/mL TSH) and  $7.1 \pm 1.7$  nM (1 mIU/mL TSH) (Fig. 2D). In the absence of TSH, only low levels of T3 were detected at the first three time points,

**Tab. 2: Relative change of T3 secretion in 3D thyroid model after methimazole (MMI) treatment**

3D thyroid models stimulated with 1 mIU/mL TSH were treated for 4 days with 0, 0.1, 1 or 10  $\mu$ M MMI in 2-day dosing intervals. Overall T3 concentrations were measured by LC-MS/MS in culture supernatants 2 and 4 days after treatment. Data are shown as means  $\pm$  SD of measured T3 levels normalized to respective non-treated controls (0  $\mu$ M MMI). Four independent thyroid donors were analyzed. LOQ indicates that no relative secretion could be calculated since T3 levels remained below the limit of quantification ( $< 0.1$  nM) after MMI treatment.

MMI ( $\mu$ M)	Time (day)	Donor 8 (n = 2) Mean (%) $\pm$ SD	Donor 9 (n = 3) Mean (%) $\pm$ SD	Donor 10 (n = 3) Mean (%) $\pm$ SD	Donor 11 (n = 3) Mean (%) $\pm$ SD
0	2	100.0 $\pm$ 28.3	100.0 $\pm$ 0.0	100.0 $\pm$ 20.6	100.0 $\pm$ 9.3
	4	100.0 $\pm$ 11.6	100.0 $\pm$ 3.8	100.0 $\pm$ 17.2	100.0 $\pm$ 11.2
0.1	2	118.1 $\pm$ 7.1	144.7 $\pm$ 11.1	53.4 $\pm$ 13.3	95.2 $\pm$ 24.9
	4	136.8 $\pm$ 19.4	110.8 $\pm$ 11.5	87.1 $\pm$ 6.4	96.2 $\pm$ 34.0
1	2	23.5 $\pm$ 9.8	65.8 $\pm$ 3.7	LOQ	LOQ
	4	43.0 $\pm$ 7.1	50.3 $\pm$ 3.8	LOQ	LOQ
10	2	10.8 $\pm$ 7.4	12.6 $\pm$ 3.0	LOQ	LOQ
	4	LOQ	LOQ	LOQ	LOQ

thereafter no T3 was detectable. In conclusion, TSH had a reproducible stimulatory effect on the secretion of T3, confirming the TSH-regulated functionality of the established 3D thyroid model in long-term *in vitro* studies.

### 3.1.5 TPO inhibition

Considering the *in vivo*-like architecture and TSH-dependent functionality, the static 3D thyroid model was considered to be an appropriate model to assess potential direct effects of test chemicals on TH levels. To establish the assay's suitability, 3D thyroid models from four human donors were pre-cultured for 3 days, followed by a 4-day treatment with non-cytotoxic concentrations (Fig. S3<sup>1</sup>) of MMI, a reference TPO inhibitor. The concentrations of MMI were 0.1, 1 and 10  $\mu$ M, and the culture medium, containing MMI, was replaced after two days. T3-secretion levels were measured in culture supernatants and normalized to DMSO-solvent control after 2 and 4 days of treatment (Tab. 2). A minimal effective concentration of 1  $\mu$ M MMI reproducibly inhibited T3-secretion for all donors tested. Maximal inhibiting effects were observed for 10  $\mu$ M MMI after 4 days, which repeatedly suppressed T3-secretion. These results indicate that the established 3D thyroid model can detect direct TH perturbations on T3 synthesis level.

### 3.1.6 Functional properties of the dynamic 3D thyroid model

Morphological characterization of 2-week dynamically cultured thyroid models reproduced spherical arrangement of the cells as previously seen under static conditions. H&E staining (Fig. 3A) visualized the follicular orientation of the cells and the presence of an intrafollicular matrix that contained TG (Fig. 3B). Like the static cultures, 3D thyroid models were cultured in the absence or presence of 0.1 or 1 mIU/mL TSH while being exposed to dynamic flow in the Chip2. T3 and T4 secretion levels were monitored. Again, the 3D thyroid model hardly secreted any

T4 in all conditions tested (Tab. S4<sup>1</sup>). While T3 could not be detected in any of the donors in the absence of TSH, TSH-treated groups maintained reproducibly stable levels of T3 from day 5 with means of  $3.8 \pm 1.8$  nM (0.1 mIU/mL TSH) and  $5.3 \pm 2.0$  nM (1 mIU/mL TSH) (Fig. 3C). No significant difference was observed between these two groups ( $p = 0.137$ , unpaired t-test). In summary, TSH-regulated functionality of the established 3D thyroid model was also found under dynamic culture conditions.

## 3.2 Characterization of HepaRG/HStcC liver spheroids

### 3.2.1 Characterization of hepatic thyroid hormone catabolism in dynamic culture

To establish a relevant *in vitro* liver system that can, in combination with the 3D thyroid model, simulate the essentials of TH homeostasis, the HepaRG/HStcC liver spheroid model needed to demonstrate key characteristics of the hepatic phenotype.

As the intracellular transport of THs and the efflux of their catabolites are fundamental requirements for hepatic TH catabolism *in vitro*, the morphology of freshly generated HepaRG/HStcC liver spheroids was analyzed. In this respect, the immunofluorescence detection of the highly specific TH carrier protein MCT8 (Friesema et al., 2003) provided first structural evidence (Fig. 4A). The expression of the tight junction protein ZO1 and the bile transporter MRP2 indicated a functional bile canaliculi network in the liver spheroids that mediates the efflux of glucuronidated and sulfated conjugates *in vivo* (Jungsuwadee and Vore, 2010) and thus is assumed to contribute to the elimination of THs (Miyawaki et al., 2012).

*In vivo*, the hepatic serum proteins albumin and TBG are considered the main TH carrier proteins that strongly influence the half-lives of THs. As a serum-free co-culture system was envisaged, the secretion of these proteins by the established HepaRG/HStcC liver spheroid model should contribute to a more physio-

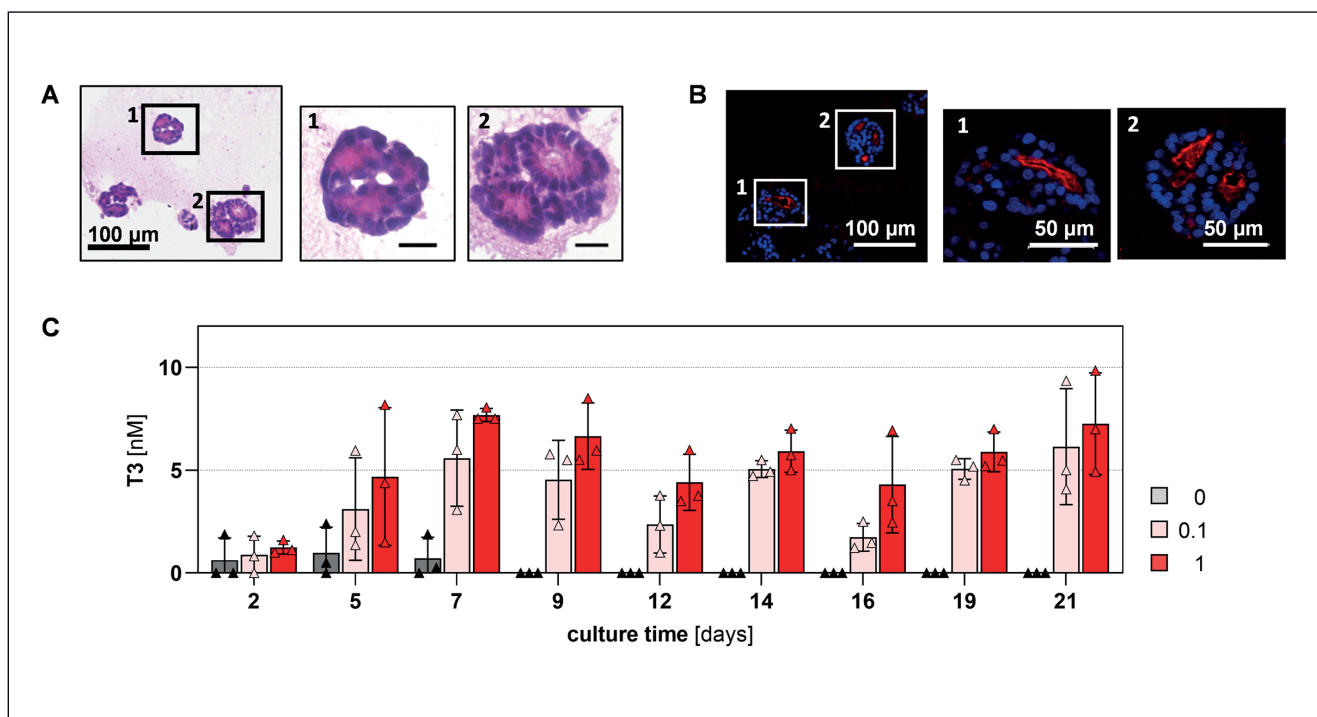


**Fig. 3: Functional characterization of the single, dynamically cultured 3D thyroid model**

(A) Hematoxylin and eosin staining of thyroid-stimulating hormone (TSH)-exposed 3D thyroid model (Donor 11) after being cultured for 15 days in the 2-organ chip platform. (1) Scale bar:  $10\ \mu\text{m}$ . (2) Scale bar:  $20\ \mu\text{m}$ . (B) Representative fluorescence images of 14-day dynamically cultured TSH-treated thyroid follicles (Donor 11). Intrafollicular colloid was visualized by immunofluorescent staining of thyroglobulin (TG, red, DyLight 594). Blue corresponds to DAPI labelling the nuclei. (C) TSH-dependent T3 secretion of 21-day dynamically cultured 3D thyroid model. Triiodothyronine (T3) was measured in culture supernatants from the 3D thyroid model exposed to 0 (grey), 0.1 (light red) or 1 (red) mIU/mL TSH by LC-MS/MS analysis. Bars represent the mean  $\pm$  SD of three independent thyroid donors ( $n = 3$ ; each triangle represents mean of intraexperimental triplicate of one donor; Donor 7, 8, 13). Data points on the x-axis indicate T3 concentrations below limit of quantification ( $< 0.5\ \text{nM}$ ).

logical TH homeostasis. 50 HepaRG/HStc liver spheroids cultured in the HUMIMIC Chip2 secreted both albumin and TBG over the whole 21-day culture. Albumin remained within a 2-fold range over time, whereas TBG concentrations fluctuated around a 3-fold range, both declining below the day 2 values at day 21 (Fig. 4B). Despite these declines, the observed viability and hepatocyte-specific functionality indicated the model's suitability for long-term exposure studies with putative TH disruptors.

Next, the expression profile of hepatic marker genes of TH metabolism was analyzed in freshly generated HepaRG/HStc liver spheroids (day 0) and compared to that of liver spheroids cultured for 14 days in the Chip2. No significant differences were observed ( $p > 0.05$ , multiple t-test corrected for multiple comparisons using Holm-Sidak method) (Fig. 4C). HepaRG/HStc liver spheroids stably expressed genes for all three TH carrier proteins (*albumin*, *TBG* and *TTR*), main cytochrome P450-enzymes (*CYP 1A1/1A2/2B6/3A4*), sulfotransferases (*SULT 1A1/1B1/1E1/2A1*), UDP-glucuronosyltransferases (*UGT 1A1/1A6/1A9/2B7*), nuclear xenobiotic receptors *CAR* and *PXR*, the nuclear TH receptor  $\beta$  (*THR $\beta$* ), two major TH transporters *NTCP* and *MCT8*, as well as *DIO1* converting T4 to T3.

### 3.2.2 gT4 and sT4 metabolite formation in static and dynamic culture

To demonstrate an active TH catabolism in HepaRG/HStc liver spheroids, their gT4 and sT4 formation was pre-characterized under static culture conditions after addition of  $1\ \mu\text{M}$  T4 on day 9. To examine accumulation of T4 metabolites over time, cell culture supernatants were analyzed after 4, 16 and 24 h of T4 addition. As expected, longer incubation periods led to an increased enrichment of the gT4 and sT4 metabolites in the culture supernatants (Fig. 4D). Selecting an exposure time of 24 h, the concentration-dependent effect of 5, 100 and 1000 nM T4 was evaluated on gT4 and sT4 formation level (Fig. 4E). Only the highest tested concentration of  $1\ \mu\text{M}$  T4 resulted in detectable amounts of both gT4 (10.8 nM) and sT4 (2.3 nM). Adapting these optimized assay conditions, HepaRG/HStc liver spheroids were cultured for 11 days in the Chip2 until being exposed to  $1\ \mu\text{M}$  T4 for 72 h (instead of the 24 h used before) to additionally increase T4 metabolite accumulation. A reproducible gT4 and sT4 formation of 10.35 nM and 6.5 nM, respectively, was found under dynamic conditions (Fig. 4F). In conclusion, the established liver spheroid model maintains meaningful features that contribute to

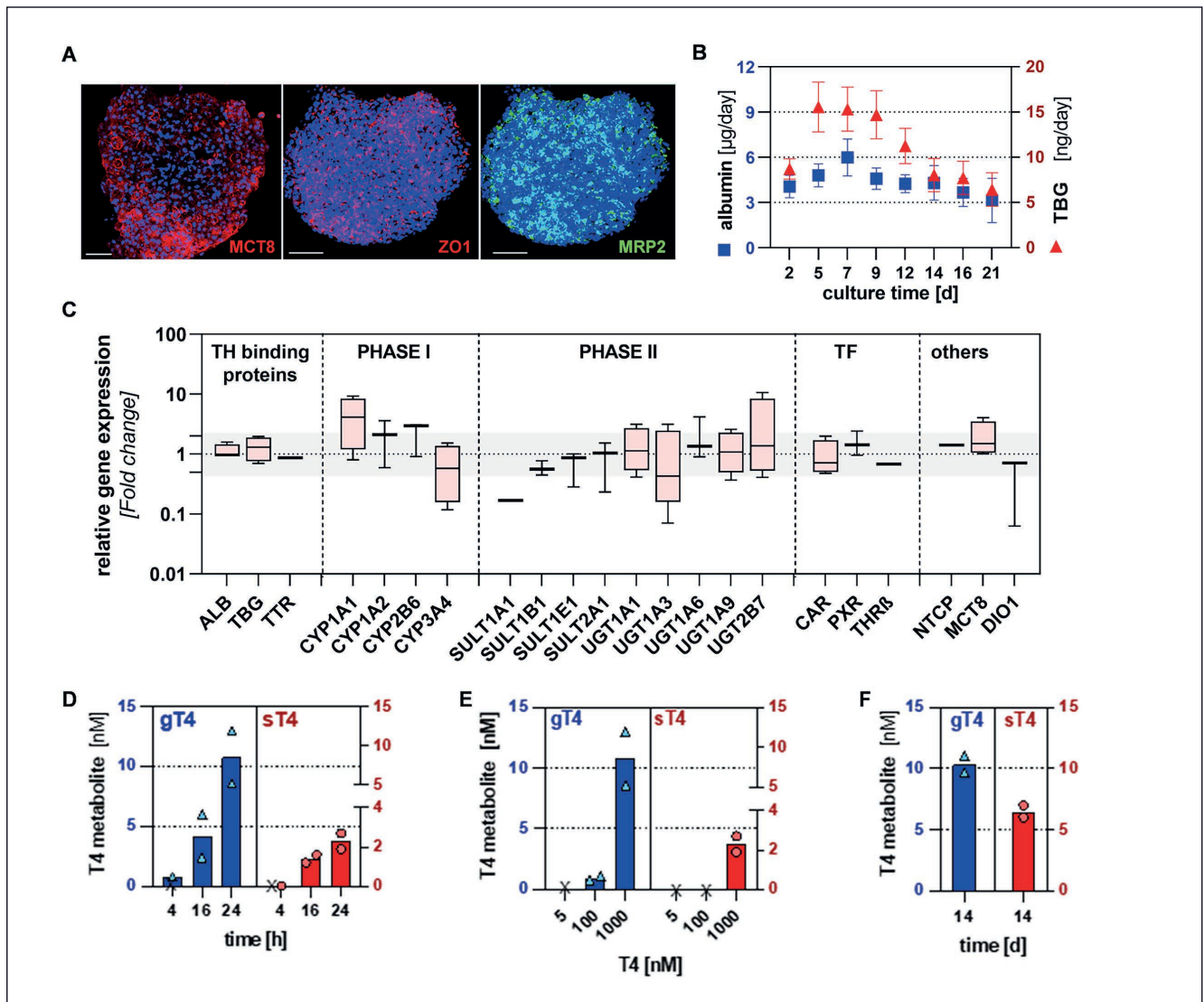


**Fig. 4: Thyroid hormone metabolism-relevant characterization of 3D HepaRG liver spheroids cultured in Chip2**

(A) Confocal laser-scanning microscopy confirms expression of the monocarboxylate transporter 8 (MCT8, red), tight junction marker ZO1 (red), and the canalicular efflux transporter MRP2 (green) prior to dynamic culture. Nuclei stained with DAPI. Scale bar: 50  $\mu\text{m}$ .

(B) Secretion of thyroid hormone carrier proteins albumin (blue, square) and thyroxine-binding globulin (TBG, red, triangle) over 21 days in dynamic culture. Data shown as mean  $\pm$  SD of two independent experiments containing three intraexperimental replicates.

(C) Fold change of genes involved in hepatic thyroid hormone (TH) metabolism after a two-week dynamic culture (d14) normalized to day 0. Grey area indicates fold changes between 0.5 and 2, which are of minor relevance. Succinate dehydrogenase complex flavoprotein subunit A (SDHA) served as a housekeeper. Differences between d0 and d14 were evaluated for each gene by multiple t-test using Holm-Sidak's post hoc test and delta Ct values for  $n > 2$ . None of the means were significantly different from the d0 control for  $p < 0.05$  and  $\text{FC} \in \text{R}0 \cup [0.5; 2]$ . ALB, albumin,  $n = 4$ ; CAR, constitutive androstane receptor,  $n = 4$ ; CYP, cytochrome P450: CYP1A1,  $n = 4$ ; CYP1A2,  $n = 2$ ; CYP2B6,  $n = 3$ ; CYP3A4,  $n = 4$ ; DIO1, human type 1 iodothyronine deiodinase,  $n = 3$ ; MCT8, monocarboxylate transporter 8,  $n = 4$ ; NTCP, sodium/bile acid cotransporter,  $n = 1$ ; PXR, pregnane X receptor,  $n = 3$ ; SULT, sulfotransferase: SULT1A1,  $n = 1$ ; SULT1B1,  $n = 3$ ; SULT1E1,  $n = 3$ ; SULT2A1,  $n = 3$ ; TBG, thyroxine-binding protein,  $n = 4$ ; THR $\beta$ , thyroid hormone receptor  $\beta$ ,  $n = 2$ ; TTR, transthyretin,  $n = 1$ ; UGT, UDP-glucuronosyltransferase: UGT1A1,  $n = 4$ ; UGT1A3,  $n = 4$ ; UGT1A6,  $n = 3$ ; UGT1A9,  $n = 4$ ; UGT2B7,  $n = 4$ .

(D-F) Overall formation of glucuronidated (gT4, blue) and sulfated (sT4, red) thyroxine from added T4 is dependent on (D) incubation time when medium is supplemented with 1  $\mu\text{M}$  T4, (E) varies in dependency of applied T4 concentrations after an incubation time of 24 h, and (F) still takes place after 14 days dynamic cultivation of the HepaRG liver spheroids in the Chip2 (24 h incubation with 1  $\mu\text{M}$  T4). gT4 and sT4 concentrations were assessed by LC-MS/MS from culture supernatants. Data are shown as mean of 2 replicates within one experiment. Data symbol X indicates values below limit of quantification (sT4 < 0.5 nM; gT4 < 0.5 nM).

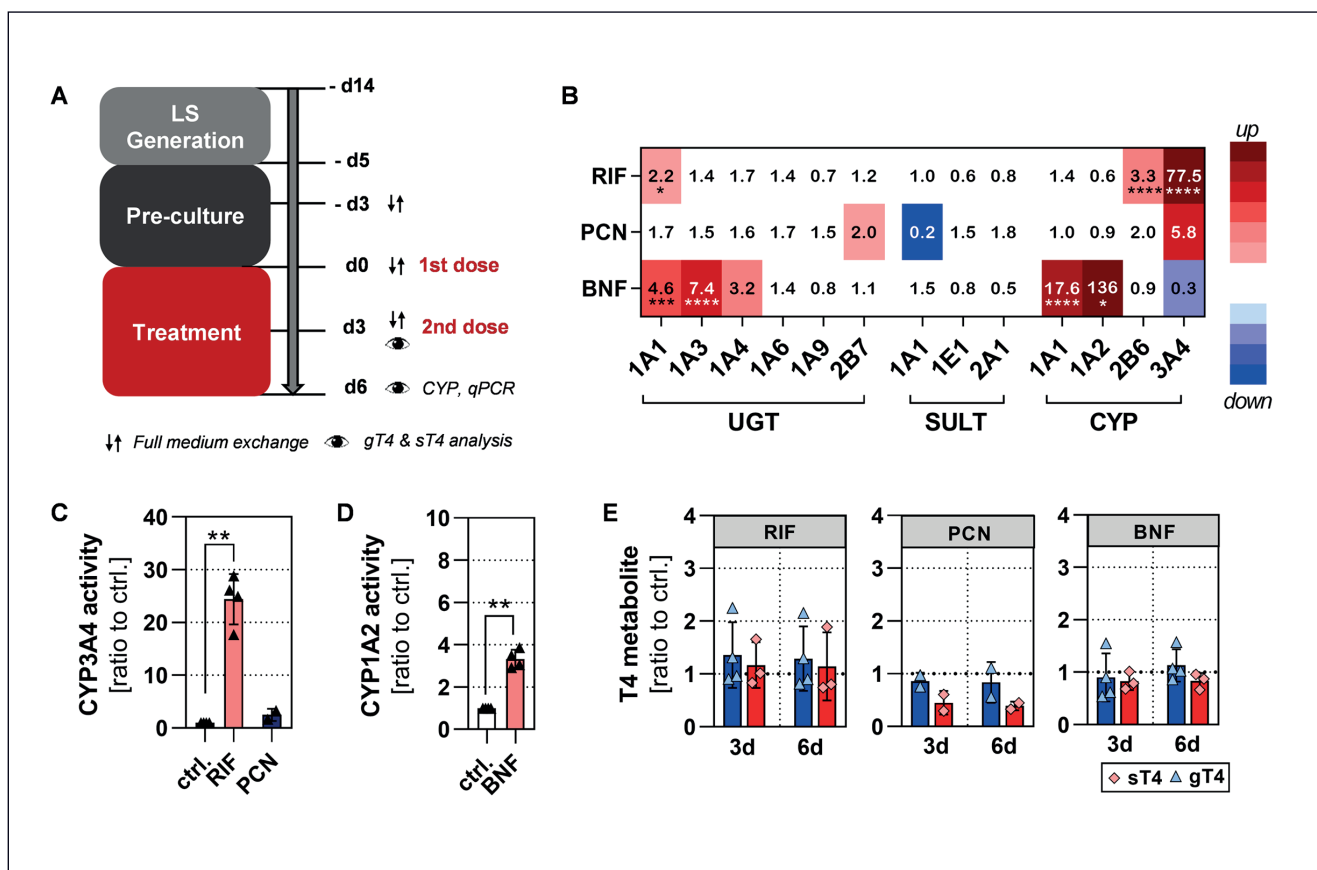


**Fig. 5: 6-day exposure of statically cultured HepaRG/HStcC liver spheroids to reference compounds significantly affects cytochrome P450 enzyme activity but rarely T4 metabolite formation**

(A) Experimental time course of a 6-day exposure to 10  $\mu$ M rifampicin (RIF), 10  $\mu$ M pregnenolone-16 $\alpha$ -carbonitrile (PCN), and 10  $\mu$ M  $\beta$ -naphthoflavone (BNF) including dosing of test compounds and artificial T4 addition at experimental day 0 and 3. (LS, liver spheroids) (B) Effect of 6-day substance exposure on mRNA expression profile of phase I and II enzymes. Succinate dehydrogenase complex flavoprotein subunit A (SDHA) served as housekeeper. Numbers indicate geometric means of the fold change calculated to solvent control (0.1% DMSO),  $n = 3$  (RIF),  $n = 2$  (PCN),  $n = 3$  (BNF). Differences between control and BNF were evaluated for each gene by multiple t-test using Holm-Sidak's post hoc test of log-transformed fold changes. Differences were considered significant for  $p < 0.05$  and  $FC \in R_{0+}[0.5; 2]$  (\*,  $p < 0.05$ ; \*\*,  $p < 0.001$ ; \*\*\*,  $p < 0.0001$ ). CYP, cytochrome P450; SULT, sulfotransferase; UGT, UDP-glucuronosyltransferase (C) Fold induction of CYP3A4 activity in response to RIF ( $n = 4$ ) and PCN ( $n = 2$ ), and of (D) CYP1A2 in response to BNF ( $n = 4$ ) normalized to solvent control (ctrl.). For comparison, differences were evaluated via an unpaired t-test using Welch's correction and considered significant for  $p < 0.05$  (\*\*,  $p < 0.01$ ). (E) gT4 and sT4 metabolite levels were quantified in culture supernatants after 3 and 6 days RIF, PCN or BNF exposure via LC-MS/MS analysis. Depicted are the average ratios to solvent control. Data are shown as mean  $\pm$  SD of  $n = 2$  to 4. Differences to the control were evaluated by two-way ANOVA followed by Sidak's multiple comparison post-hoc test for  $n > 2$  ( $p < 0.05$ ) with none of them being significant.

an *in vivo*-like TH homeostasis while demonstrating for the first time an active TH catabolism in HepaRG-based liver spheroids in the Chip2.

### 3.2.3 Effect of RIF, PCN, and BNF on CYP P450 activity and gT4/sT4 formation under static conditions

Nuclear receptor activation of AHR and PXR are considered relevant MIEs to induce liver phase II enzymes and thereby increase the catabolism of THs (Noyes et al., 2019). Based on albumin production, a sensitive hepatic indicator of cytotoxicity

(Kühnl et al., 2021), the applied concentrations of the nuclear receptor-activating compounds were demonstrated to be non-cytotoxic (Fig. S4<sup>1</sup>).

In a first study, the inducibility of phase I and II liver enzymes was pre-characterized in HepaRG/HStcC liver spheroids under static conditions. Gene expression changes normalized to the solvent control after a 6-day treatment with RIF, PCN, and BNF are depicted in Figure 5B. *UGT1A1* ( $p = 0.0336$ ), *CYP2B6* ( $p < 0.0001$ ), and *CYP3A4* ( $p < 0.0001$ ) were found to be significantly upregulated by RIF treatment whereas no significant

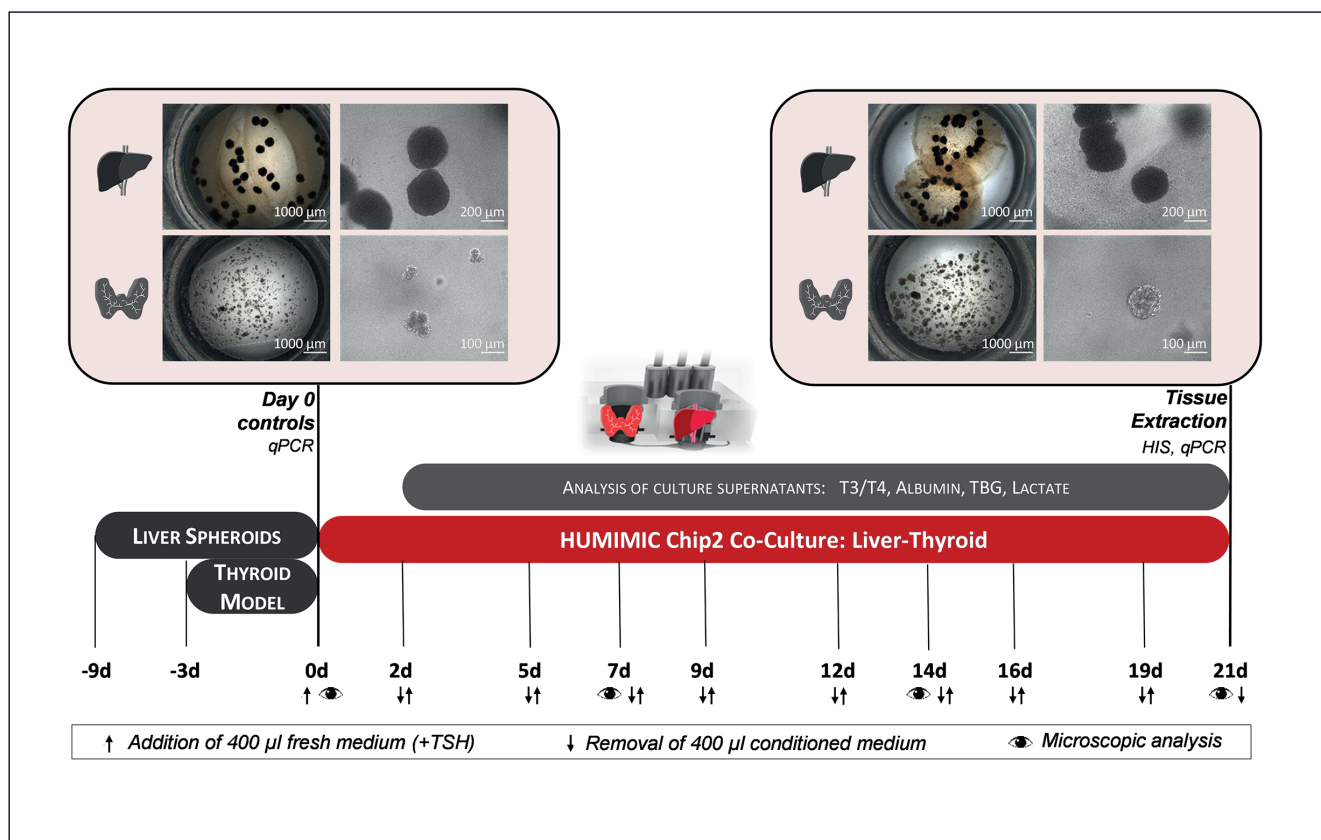


**Fig. 6: Experimental design of the co-culture process of 3D liver and thyroid models in the Chip2**

Overview depicts the timeline of the pre-culture and subsequent co-culture process with time points for in-process analysis and sampling of day 0 controls and endpoint analysis. HIS, histology, qPCR, quantitative polymerase chain reaction, T3, triiodothyronine, T4, thyroxine, TBG, thyroxine-binding globulin. Microscopic pictures show representative bright field images of organ models at 2 x and 10 x (liver) or 20 x (thyroid) magnification at the beginning and end of the chip culture.

changes in gene expression were detected for PCN. BNF exposure resulted in significant upregulation of *UGT1A1* ( $p = 0.0002$ ), *UGT1A3* ( $p < 0.0001$ ), *CYP1A1* ( $p < 0.0001$ ), and *CYP1A2* ( $p < 0.0001$ ).

To evaluate these transcriptomic inductions on phase I and II enzyme activity level, compound-dependent changes in CYP3A4/1A2 activities and gT4/sT4 formation were analyzed in HepaRG/HStEC liver spheroids represented in Figure 5C, D and E, respectively. Coherent with mRNA expression levels, 6-day treatment with RIF caused a 24.4-fold increase in CYP3A4 activity ( $p = 0.0022$ ). No relevant changes in basal CYP3A4 activity were detected for HepaRG/HStEC liver spheroids following PCN treatment. BNF significantly induced CYP1A2 activity 3.3-fold ( $p = 0.0017$ ). Despite the demonstrated effects of RIF and BNF on UGT gene expression and CYP activity, the compounds did not affect T4 glucuronidation after 3 or 6 days. No change was observed in the amount of secreted sT4 after the RIF or BNF treatment, which is in line with the observed unchanged *SULT* gene expression levels. In contrast, the 6-day treatment with PCN resulted in decreased sT4 formation, as reproducibly shown in two independent experiments.

In summary, HepaRG/HStEC liver spheroids were found to respond to AHR and PXR agonists with transcriptomic changes of UGT and CYP enzymes as well as induction of CYP enzyme activities. In contrast, these hepatic nuclear receptor activations did not show any effect on the sT4 and gT4 formation rate in the HepaRG/HStEC liver spheroids.

Similar observations were made when HepaRG/HStEC liver spheroids were treated with RIF in the Chip2. Only inductive effects on CYP enzyme activity level were observed without affecting UGT-T4 or *SULT*-T4 activities (Fig. S5<sup>1</sup>), confirming the data obtained under static conditions.

### 3.3 Combining the 3D thyroid model and HepaRG/HStEC liver spheroids in a Chip2 for 21 days

Having established a functional 3D thyroid model and HepaRG/HStEC liver spheroid model, which simulate both the biosynthesis and catabolism of THs, the combination of the two tissues was undertaken in a multi-organ chip platform, the Chip2. Being composed of two culture compartments, each the size of a standard 96-well, the integrated organ models are spatially separated while a microfluidic channel system allows their metabolic ex-

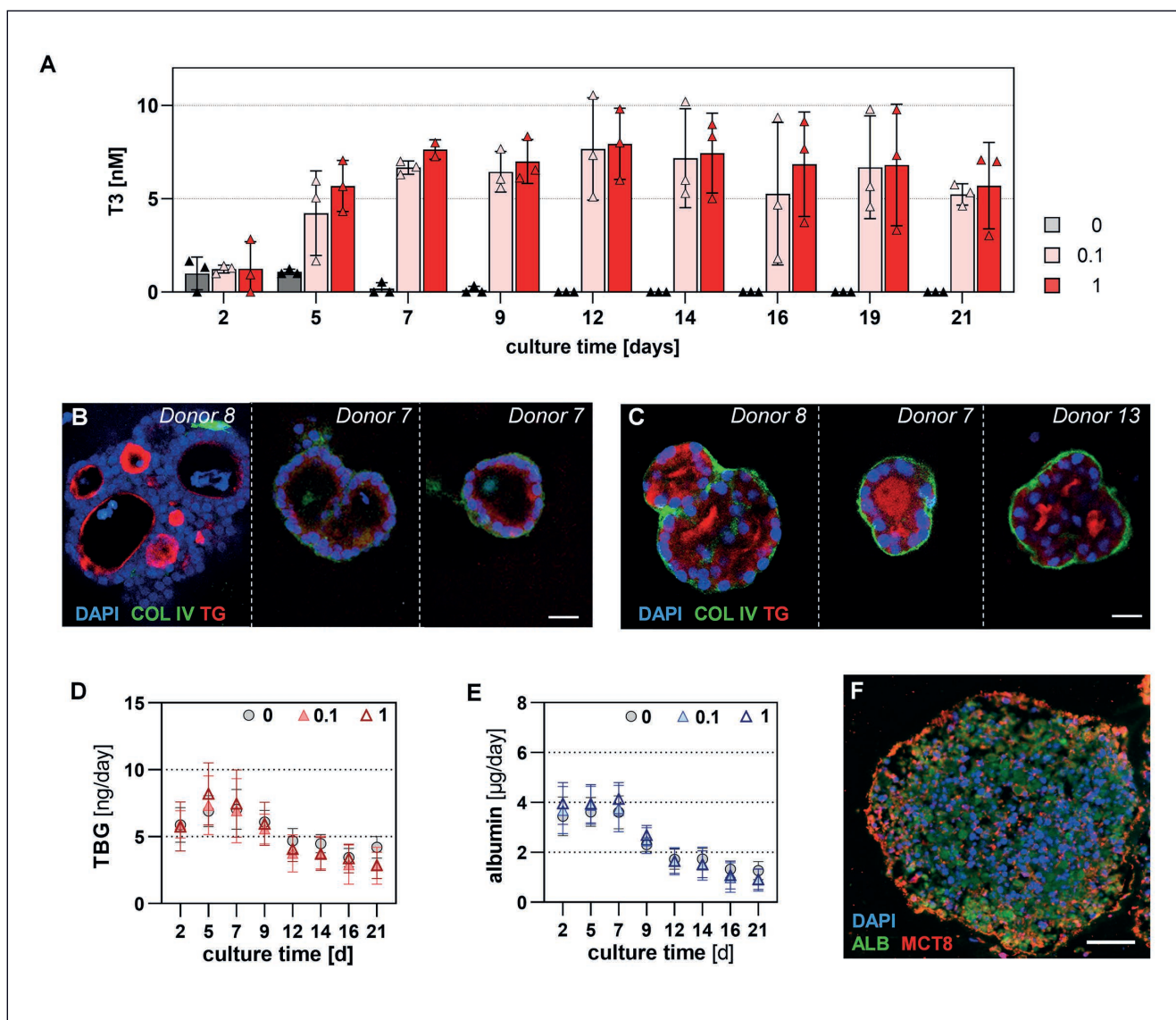


**Fig. 7: 3D liver and thyroid models stay functional in dynamic co-culture over 21 days**

(A) TSH-dependent triiodothyronine (T3) secretion of 21-day dynamically co-cultured thyroid model. T3 was measured in culture supernatants from co-cultures exposed to 0 (grey), 0.1 (light red), and 1 (red) mIU/mL TSH by LC-MS/MS analysis. Bars represent the mean  $\pm$  SD of three independent thyroid donors ( $n = 3$ ; one triangle/donor). Data points at x-axis indicate values below limit of quantification ( $< 0.5$  nM). (B, C) Morphological analysis of thyroid models co-cultured for 21 days (B) without or (C) with 1 mIU/mL TSH by whole tissue staining of the colloidal glycoprotein thyroglobulin (TG, red, DyLight 594), the basal lamina protein collagen IV (Col IV, green, DyLight 488), and the cell nuclei (DAPI, blue). Scale bars:  $20 \mu\text{m}$ . Numbers indicate different donors. (D, E) Serum proteins thyroxine-binding globulin (TBG, (D)) and albumin (E) levels in conditioned medium were periodically analyzed and depicted as the total produced protein amount per day. Data shown as mean  $\pm$  SD for each co-culture condition (w/o TSH (0) or with 0.1 mIU/mL TSH or 1 mIU/mL TSH) ( $n = 3$ ). (F) Protein expression of thyroid hormone carrier protein albumin (green) and thyroid hormone transporter MCT8 (red) at day 21 in co-culture. Nuclei stained with DAPI (blue). Scale bar:  $100 \mu\text{m}$ . Thyroid models for co-culture were derived from Donor 7, 8 and 13.

change (Fig. 1B). An on-chip micropump, operated by a pressure/vacuum of  $\pm 300$  mbar at a frequency of 0.45 Hz, generated an average flow rate of  $2.15 \mu\text{L}/\text{min}$ , which enabled a complete medium turnover within  $\sim 2.5$  h. The liver model, represented by 50 HepaRG/HStc liver spheroids, and the 3D thyroid model, com-

posed of 1000 thyroid follicles, were co-cultured over 21 days under chemically defined, serum-free conditions according to Figure 6. To evaluate the reproducibility of the assay, co-cultures with three independent human thyroid donors were performed. Co-cultures were stimulated with 0, 0.1 or 1 mIU/mL TSH.

Comparing the thyroid-specific readouts, a reproducible organ-level functionality similar to the single-culture was found. From day 5, the co-cultures showed stable, reproducible T3 levels in the presence of TSH with mean levels of  $6.2 \pm 1.2$  nM (0.1 mIU/mL TSH) and  $6.9 \pm 0.8$  nM (1 mIU/mL TSH) on the day of medium exchange being not significantly different from each other (Fig. 7A). The TSH-negative group did not reveal any measurable amounts of T3 from day 7 on (LOQ < 0.5 nM). As observed in thyroid single culture, no T4 was detected in culture supernatants under any condition. Consequently, the hepatic TH catabolites gT4 and sT4 were not detected either. Immunohistological staining of the stimulated and unstimulated 3D thyroid model revealed a similar TSH-dependent morphology after co-culture as previously described for single-cultured thyroid models under static conditions (Fig. 7B,C).

Similar to the previous hepatic single cultures, the TBG (Fig. 7D) and albumin (Fig. 7E) levels decreased after 9 days of co-culture, but the effect was more pronounced in the dynamic culture. There was a trend towards more stable values towards the end of the culture, with no apparent differences between the TSH-exposure groups. Despite the decreased secretion of serum proteins, the hepatic phenotype was maintained. Cells throughout the whole spheroid clearly demonstrated albumin expression at the end of the 21-day co-culture (Fig. 7F). Simultaneously, the expression of the MCT8 transport protein was confirmed. Furthermore, gene expression profiles of hepatic marker genes of 21-day co-cultured liver spheroids were similar to freshly generated and 21-day single-cultured liver spheroids. Apart from *CYP3A4*, solely shown to be downregulated after co-culture, albumin, *MRP2*, *BSEP* (bile salt export pump), *SLC10A1* (solute carrier known to transport THs (Friesema et al., 2005)), *UGT1A1*, and *SULT1A1* mRNA expression levels were maintained under all conditions and respectively confirmed a maintained hepatic phenotype of the co-cultured liver spheroids (Fig. S6<sup>1</sup>).

In summary, this study presents a first proof of concept for a functional combination of human 3D liver and thyroid models over a period of 21 days. This organ-on-a-chip model might, in the future, provide a powerful *in vitro* tool to study thyroid homeostasis on a next level of human relevance addressing aspects of organ-organ interaction.

## 4 Discussion

Assessing the human relevance of safety-related findings in rodents with respect to thyroid toxicity is key during the development of new PPPs. This study presents a new approach methodology (NAM) aiming to investigate the human safety of these chemicals by addressing potential thyroid adverse effects at a functional level using tissues from the relevant species. To this end, a human-based co-culture of 3D thyroid and liver organ models was established that can be cultured for 21 days. This culture time is assumed to be long enough to allow meaningful mechanistic investigations (e.g., nuclear receptor activation, changes in hepatic enzyme activity) as demonstrated in 7-day

mechanistic short-term studies in rats (Tinwell et al., 2014). In depth pre-characterization of the statically cultured single organ models indicated the suitability of the 3D thyroid model to detect direct TH inhibitors and provided evidence of an active TH catabolism in HepaRG/HStEC liver spheroids. Accordingly, the individually cultured organ models are already of value to investigate organ-specific mechanisms of TH homeostasis and related toxicities.

### 4.1 Detection of direct thyroid hormone perturbation with the 3D thyroid model

We established a functional human 3D thyroid model derived from tissue-recovered primary thyroid follicles and GFR Matrigel as a structural matrix that is suitable for static and dynamic culture conditions.

Major features of the 3D thyroid model presented here are its physiological and structural characteristics, as TSH-responsive morphology is maintained for 21 days in both culture formats. From earlier reports, it is known that ECM components are key to promoting a thyroid-specific phenotype *in vitro*, reinforcing the native polarization of thyrocytes (Chambard et al., 1984; Mauchamp et al., 1998). As demonstrated by our results, the 3D thyroid model maintained the typical basolateral cell polarization, showing follicle-surrounding collagen IV expression that is known to be a major component of the basement membrane in human thyroid tissue (Bürgi-Saville et al., 1997). The interior of the *in vitro*-cultured follicles was filled with TG, which is utilized by apical/luminal expressed enzymes such as TPO to synthesize THs *in vivo* (Mondal et al., 2016). This arrangement indicates intrafollicular apical cell polarization, which in turn is suggestive of functional TH biosynthesis. Remarkably, continuous TSH-stimulation resulted in morphologic changes of the *in vitro*-cultured follicles that correlate well with the concept of active and resting follicles showing a high or low level of TH synthesis, respectively (Dumont, 1971; Yuri et al., 2018). *In vivo*, the appearance of active follicles, most prominently during hyperplasia, is characterized by a columnar morphology, whereas cells of resting ones reveal a cuboidal shape and a more abundant colloid (Yuri et al., 2018), which is in agreement with our results. In summary, our findings indicate that thyroid hyperplasia and hypertrophy can be mimicked in our model.

According to EFSA, the most prominent direct thyroid effects are the blockage or competitive inhibition of iodine uptake via sodium-iodide symporter (NIS) and the reversible or irreversible inhibition of TPO (Crivellente et al., 2019). For early pipeline molecules, these MIEs can be addressed using currently available high-throughput assays (Noyes et al., 2019). However, such approaches are lacking in physiological relevance, as they are based on cell-free environments (Murk et al., 2013) or transfected human cell lines such as hNIS-HEK293T-EPA (Wang, J. et al., 2019).

Here, we present a human 3D thyroid model that offers TH secretion as a functional marker for the *in vitro* evaluation of direct thyroid toxicity. The results of our study demonstrated a stable release of T3 in the presence of TSH over 21 days for statically as well as dynamically single-cultured thyroid folli-



cle models. *In vivo* T3 plasma concentrations in healthy human subjects range from 1.0 to 3.0 nM (Gardas, 1991; Hohtari et al., 1987); the *in vitro* achieved concentrations of  $\sim 3.8 \pm 1.8$  nM (0.1 mIU/mL TSH, dynamic single-culture) are consistent with these levels. However, in contrast to the *in vivo* situation, our 3D thyroid models demonstrate low to zero T4 secretion, which *in vivo* represents the major product of TH synthesis and is 16.8-times more abundant than T3 (Pilo et al., 1990). Even though some known 3D thyroid models were shown to secrete T4 (Deisenroth et al., 2020; Spinel-Gomez et al., 1990), none of these have reproduced the physiological T4/T3 ratio, even if T4 was the dominant TH. Massart et al. (1988) even demonstrated a significant decrease of T4 levels when their thyroid follicle cultures were supplemented with TSH. In this respect, it was hypothesized that type I and type II deiodinase (DIO1 and 2), both strongly expressed in thyroid tissue (Uhlén et al., 2015), contribute to the decreased T4 levels as they mediate the conversion of T4 into T3 in a TSH-dependent manner (Deisenroth et al., 2020; Massart et al., 1988; Mondal et al., 2016; Murakami et al., 2001). Supporting this hypothesis is the observation that patients with T3-predominant Grave's disease are characterized by an increased free T3/T4 ratio, which is attributed to elevated DIO1/2 activity (Ito et al., 2011).

Despite the low levels of T4, T3 secretion under TSH stimulation could be suppressed by MMI, a reference TPO inhibitor (Friedman et al., 2016). For a proof of concept, statically cultured 3D thyroid models from four different donors were exposed to MMI. After 2 and 4 days, a reproducible decrease in T3 could be observed for 1  $\mu$ M and even stronger for 10  $\mu$ M MMI. These values correlate well with maximal observed serum concentrations of MMI ( $2.61 \pm 0.81$   $\mu$ M) when a daily dose of 10 mg MMI is administered to patients with hyperthyroidism (Okamura et al., 1986). Additionally, a similar range of effect concentrations of MMI were previously reported when human TPO activity was measured directly in TPO extracts from Nthy-ori 3-1 cell line ( $IC_{50}$  2.7 - 4.0  $\mu$ M) (Jomaa et al., 2015), primary tissue (0.8-2  $\mu$ M) (Nagasaka and Hidaka, 1976), and *ex vivo* treated thyroid slices ( $IC_{50}$  5.0  $\mu$ M) (Vickers et al., 2012). Notably, our results are in line with a recently published human 3D thyroid model in which 1  $\mu$ M MMI was reported to be the lowest concentration at which changes in TH secretion were observed (Deisenroth et al., 2020). Taken together, the established 3D thyroid model was able to identify one of the most prominent MIEs for adverse thyroid-mediated outcomes, namely TPO inhibition.

Furthermore, this data provided evidence that the secreted T3 is the product of a *de novo* TH synthesis, since active TPO enzymes are evidently required for *in vitro* TH synthesis, and is not a result of a TSH-induced liberation from an internal T3 reservoir as previously described for thyrocyte monolayer cultures (Ollis et al., 1985). The latter might explain the secretion of T3 in the TSH-non-induced state. Nevertheless, it must be noted that our TH-inhibition study was conducted under static culture conditions only. Future studies therefore will examine the reproducibility of the results when the 3D thyroid model is exposed to MMI under dynamic flow in the HUMIMIC Chip2.

Our human 3D thyroid model presents the first *in vitro* thyroid model that can be incorporated into a perfused organ-chip system with viability and TSH-dependent T3 secretion over 21 days. The use of a commercially available multi-organ chip platform, quality-controlled according to ISO 9001-2015 standards, ensures the robustness of the underlying equipment background and the corresponding chip culture ware. Various assay formats applying different human organ models have been qualified previously on this platform by pharmaceutical companies in other contexts of use (Marx et al., 2020). This knowledge fed into the establishment of a reproducible thyroid-liver co-culture. However, further refinement of the model must be considered if one wants to achieve the physiological T4/T3 ratio by, for example, understanding and monitoring the activity of DIO1/2 in the system. So far, only the gene expression of DIO1 was analyzed and showed no striking difference compared to expression levels in primary tissue (Fig. S7<sup>1</sup>).

#### 4.2 HepaRG/HStcC liver spheroids as a tool for evaluating hepatic thyroid hormone catabolism

There is an urgent need to set up models that can simulate human hepatic TH metabolism *in vitro* and thus increase our understanding of the relevance of xenobiotic-related euthyroid effects observed in rodents for humans. Recent advances point towards 3D hepatocyte spheroid models, which maintain and even improve the liver-specific phenotype over longer periods of time compared to 2D cultures (Bell et al., 2016; Cox et al., 2020; Lauschke et al., 2016; Underhill and Khetani, 2018). In particular, 3D cultures of HepaRG cells, which are already considered a good surrogate for primary human hepatocytes (Aninat et al., 2006; Hoekstra et al., 2013; Huaman et al., 2012; Kammerer and Küpper, 2018; Lübberstedt et al., 2011; Tascher et al., 2019), are able to compensate known limitations of monolayer cultured HepaRG cells, e.g., by inducing urea formation (Gaskell, 2016; Gunness et al., 2013; Li et al., 2019) and enhancing CYP2E1 activity (Gunness et al., 2013). We characterized HepaRG/HStcC liver spheroids as a suitable model to study hepatic T4 metabolism and their potential to evaluate liver-mediated thyroid toxicity. To our knowledge, neither the HepaRG cell line nor related 3D liver models have been characterized with regard to their TH metabolism previously.

*In vivo*, the hepatic serum-binding proteins are key for the overall transport of THs and represent their main storage capacity since they bind up to 99.5% of total T3 and T4 (EC, 2017). Even if albumin is the most abundant serum protein in humans, TBG binds 75% of the majority of THs (Janssen and Janssen, 2017). This is the first study showing that HepaRG/HStcC liver spheroids in Chip2 culture can produce TBG over a 3-week period and thus can contribute to the TH homeostasis when co-cultured with the 3D thyroid model. For future assay refinement, this newly characterized read-out parameter could serve to evaluate xenobiotic-induced TH displacements or protein abnormalities that are associated with altered TH levels. Together with the stable albumin production, which was previously demonstrated in chip-cultures and serves as an overall hepatic functionality marker (Bauer et al., 2017; Schimek et al., 2020), a prolonged

culture of the HepaRG/HStcC liver spheroids can be assumed, allowing long-term studies and repeated exposures to mimic *in vivo* treatments.

THs and their metabolites rarely pass the plasma membrane via diffusion, but require active uptake and excretion via transport proteins (Visser et al., 2011). We were able to demonstrate the expression of MCT8, a highly specific TH-transporter (Visser et al., 2011), and the bile transporter MRP2, generally known to mediate the excretion of glucuronidated and sulfated conjugates (Jungsuwadee and Vore, 2010), at protein level in freshly generated HepaRG/HStcC liver spheroids and its transcriptomic stability after 14 or 21 day chip-culture. Most importantly, however, was the transcriptomic evidence of *UGT 1A1/1A3/1A9* and *SULT 1A1/1B1/1E1*, which have been described as having a TH-specific activity in humans (Findlay et al., 2000; Gamage et al., 2006; Kato et al., 2008; Kester et al., 1999). Accordingly, HepaRG/HStcC liver spheroids represented fundamental features required for active TH uptake, the metabolization of THs via respective UGT and SULT enzymes, and the efflux of the generated glucuronidated and sulfated TH metabolites. The relevance of these findings was finally confirmed by the active formation of gT4 and sT4 metabolites in 14-day dynamically cultivated HepaRG/HStcC liver spheroids. To the best of our knowledge, this study presents a dynamic 3D liver model that can mimic hepatic T4 catabolism *in vitro* for the first time.

Similar to Richardson et al., who verified basal T4 catabolism in static sandwich-cultured human hepatocytes between culture day 3 to 6 after applying 0.1  $\mu\text{M}$  T4 (Richardson et al., 2014), the gT4 and sT4 formation of our static model increased with T4 concentration and duration of T4-exposure. However, in our assay set-up, measurably stable gT4 and sT4 secretion levels were only detectable at T4 concentrations  $\geq 1 \mu\text{M}$ , which is above the physiological range of T4 (54–160 nM) (Gardas, 1991; Hohtari et al., 1987) and the expected T3/T4 secretion levels, which is a limitation of the present model. However, the addition of isotope-labelled T4 could be considered to measure impairments of TH catabolite formation as an endpoint during future studies with thyroid-liver co-cultures, which would allow to discriminate between secreted and supplemented T4, as successfully demonstrated by Karwelat et al. (2022) using a rat thyroid-liver chip model.

In our study, we indirectly demonstrated the activation of the hepatic nuclear receptors PXR and AHR in statically cultured HepaRG/HStcC liver spheroids while simultaneously analyzing their TH catabolism via the formation of gT4 and sT4. To prove the functional integrity of the liver model, the inducibility of the two major phase I biotransformation enzymes CYP1A2 and CYP3A4 was demonstrated by BNF and RIF, respectively. Induction levels of CYP1A2 activity were slightly lower than previously published results, however, shorter induction times with BNF and different analytical methods might be the reason for the observed differences (Leite et al., 2012; Lübberstedt et al., 2011). In contrast, the extent of CYP3A4 induction mediated by RIF correlated well with previous findings in 3D HepaRG liver spheroids (Aninat et al., 2006; Desai et al., 2017). As expected, PCN proved to be ineffective in human cells, whereas in rodents

it is known to lead to CYP3A induction (Karwelat et al., 2022; Xie et al., 2000). Thus, the established HepaRG/HStcC liver spheroid model appears to respond to AhR and human-specific PXR activation of phase I enzymes under static conditions.

Even though the activation of these hepatic nuclear receptors is considered a potential MIE, causing impairment of the TH system (Noyes et al., 2019), neither of them was able to significantly increase basal TH catabolite formation. In conclusion, the relationship between nuclear receptor activation and TH catabolism via phase II enzyme activity induction could not be shown for the statically cultured HepaRG cell model despite induction of UGT phase II enzymes on gene transcript level being detected. To our knowledge, neither the effect of PCN nor BNF on hepatic phase II enzymes has been studied in humans to date. In agreement with our findings, *in vitro* 2D culture data showed no relevant changes in human T4-UGT activity after a 3-day BNF exposure (Bars et al. unpublished). Of the few available human *in vivo* studies that report RIF-related alterations of T4 serum levels without pathophysiological outcomes, none directly evaluated whether these changes could be attributed to altered gT4 and sT4 formation (Curran and DeGroot, 1991; Meek et al., 2003; Ohnhaus and Studer, 1983). Although gT4 and sT4 synthesis were not affected in our studies, RIF and BNF significantly induced mRNA levels of UGTs associated with T4 activity, supporting the activation of the nuclear receptors, PXR and AHR. mRNA levels of analyzed SULT enzymes remained stable, confirming that no effects on sT4 synthesis level were to be expected. The discrepancies between mRNA expression level and UGT enzyme activity, however, are not surprising as they have been reported previously (Ohtsuki et al., 2012). Conclusions taken from this data strengthen the theory that nuclear receptor activation has less relevance to hepatic TH catabolism in humans.

In contrast, an equivalent assay that we have recently established for the rat showed distinct effects of PCN and BNF on gT4 formation (Karwelat et al., 2022). However, whether the observed differences between these assays, representing human and rat, have *in vivo* relevance remains to be further investigated. Due to insufficient reference data, it is difficult to verify how representative the HepaRG-derived model is. In a 2D sandwich-cultured human primary hepatocyte model, an increase in gT4 formation was detected following a 72 h treatment with PCB 153, indicating that T4-UGT activation is already detectable at incubation periods of 3 days and, more importantly, indicating its occurrence in human primary cells (Richardson et al., 2014). In contrast to our selected model compounds, PCB 153, a phenobarbital-like inducer, is known to be an activator of the constitutive androstane receptor (CAR) (Al-Salman et al., 2012), which in rodents can be accompanied by induced T4-UGT activity (Hood et al., 2003). Further mechanistic investigations of the HepaRG/HStcC liver spheroid model should therefore investigate if appropriate reference compounds can reproduce CAR induction and mediate enhanced T4 glucuronide formation. In addition, it must be considered that the currently available data serve to validate the use of statically cultured HepaRG/HStcC liver spheroids for pharmacological investigations. However, a first induction study of the model under dynamic conditions indi-



cated similar phase I and II enzyme properties as already shown for the static equivalent.

In summary, the assay described in this study serves as a proof-of-concept in which gT4 and sT4 metabolism in HepaRG/HStcC liver spheroids can be evaluated. Furthermore, it presents a transferable approach that can be easily adapted for PHH-derived spheroids which, in the future, might provide a cross-donor survey with increased human relevance.

#### 4.3 Co-culture

Having established physiologically relevant single-tissue organ-chip cultures over 21 days, the maintenance of their functionality was explored in a co-culture set-up. Here, we demonstrate a unique co-culture approach of the developed 3D thyroid model and HepaRG/HStcC liver spheroids over three weeks in which key organ functionalities were maintained similarly to those observed in single culture. Whether the decrease of albumin and TBG over time indicate a general decrease in hepatic functionality, which also affects TH catabolism, or if this is due to lower oxygen levels during co-culture (Felmlee et al., 2018), needs further clarification.

In conclusion, this approach can be regarded as a first step towards a multi-modular platform, which has the potential to simultaneously detect direct as well as hepatic-mediated impairments of human TH homeostasis. Future studies will focus on determining whether the co-culture system can detect perturbations of TH homeostasis as previously shown in static single cultures.

#### 4.4 Conclusion and perspectives

In this publication, we provide a first proof of concept towards a more complex test method that evaluates TH perturbations on a higher biological level compared to traditional assays (2D cultures, protein-ligand binding studies). We present a 3D thyroid follicle model and a 3D HepaRG/HStcC liver spheroid model that under static conditions can be used to evaluate direct as well as indirect TH perturbations with improved human relevance. The established 3D thyroid model emulated *de novo* T3 biosynthesis while maintaining a morphological as well as metabolic response towards TSH for a 21-day organ-chip culture. Direct thyroid toxicity was demonstrated by MMI via decreased T3 secretion in the statically cultured model. The HepaRG/HStcC liver model demonstrated active phase II enzymes resulting in hepatic baseline catabolism of T4 via glucuronidation and sulfation, which has not been demonstrated before.

Consequently, the work presents a first step towards a multi-modular human platform to evaluate hepatic and thyroidal associated dysregulations of TH metabolism separately or in combination. In its intended context of use, the assay has the potential to significantly contribute to the reduction and refinement of animal-based studies and to bridge the gap between data derived from initial high-throughput assays and follow-up *in vivo* animal studies. The combination of the rat-based thyroid-liver assay, which was developed in parallel (Karwelat et al., 2022), with the model presented here will contribute to a better understanding of species similarities and differences and thus signifi-

cantly improve the identification of thyroid disruptors that are relevant from a human safety perspective. Finally, this microfluidic chip-based thyroid-liver co-culture contributes towards microphysiological system-based models with increased human biological relevance, a trend identified to have a high potential to optimize drug discovery by laboratory animal-free investigative toxicology (Beilmann et al., 2019).

#### References

- Abel, E. D., Ahima, R. S., Boers, M.-E. et al. (2001). Critical role for thyroid hormone receptor  $\beta 2$  in the regulation of paraventricular thyrotropin-releasing hormone neurons. *J Clin Invest* 107, 1017-1023. doi:10.1172/JCI10858
- Abu-Absi, S. F., Hansen, L. K. and Hu, W.-S. (2004). Three-dimensional co-culture of hepatocytes and stellate cells. *Cytotechnology* 45, 125-140. doi:10.1007/s10616-004-7996-6
- Al-Salman, F. and Plant, N. (2012). Non-coplanar polychlorinated biphenyls (PCBs) are direct agonists for the human pregnane-X receptor and constitutive androstane receptor, and activate target gene expression in a tissue-specific manner. *Toxicol Appl Pharmacol* 263, 7-13. doi:10.1016/j.taap.2012.05.016
- Aninat, C., Piton, A., Glaise, D. et al. (2006). Expression of cytochromes P450, conjugating enzymes and nuclear receptors in human hepatoma HepaRG cells. *Drug Metab Dispos* 34, 75-83. doi:10.1124/dmd.105.006759
- Bartalena, L. and Robbins, J. (1992). Variations in thyroid hormone transport proteins and their clinical implications. *Thyroid* 2, 237-245. doi:10.1089/thy.1992.2.237
- Bartsch, R., Brinkmann, B., Jahnke, G. et al. (2018). Human relevance of follicular thyroid tumors in rodents caused by non-genotoxic substances. *Regul Toxicol Pharmacol* 98, 199-208. doi:10.1016/j.yrtph.2018.07.025
- Bassett, J. H. D. and Williams, G. R. (2003). The molecular actions of thyroid hormone in bone. *Trends Endocrinol Metab* 14, 356-364. doi:10.1016/S1043-2760(03)00144-9
- Bauer, S., Wennberg Huld, C., Kanebratt, K. P. et al. (2017). Functional coupling of human pancreatic islets and liver spheroids on-a-chip: Towards a novel human ex vivo type 2 diabetes model. *Sci Rep* 7, 14620. doi:10.1038/s41598-017-14815-w
- Beilmann, M., Boonen, H., Czich, A. et al. (2019). Optimizing drug discovery by investigative toxicology: Current and future trends. *ALTEX* 36, 289-313. doi:10.14573/altex.1808181
- Bell, C. C., Hendriks, D. F. G., Moro, S. M. L. et al. (2016). Characterization of primary human hepatocyte spheroids as a model system for drug-induced liver injury, liver function and disease. *Sci Rep* 6, 25187. doi:10.1038/srep25187
- Bernal, J. (2007). Thyroid hormone receptors in brain development and function. *Nat Clin Pract Endocrinol Metab* 3, 249-259. doi:10.1038/ncpendmet0424
- Bürgi-Saville, M. E., Gerber, H., Peter, H. J. et al. (1997). Expression patterns of extracellular matrix components in native and cultured normal human thyroid tissue and in human toxic adenoma tissue. *Thyroid* 7, 347-356. doi:10.1089/thy.1997.7.347
- Chambard, M., Gabrion, J. and Mauchamp, J. (1981). Influence of collagen gel on the orientation of epithelial cell polarity: Follicle

- formation from isolated thyroid cells and from preformed monolayers. *J Cell Biol* 91, 157-166. doi:10.1083/jcb.91.1.157
- Chambard, M., Verrier, B., Gabrion, J. et al. (1984). Polarity reversal of inside-out thyroid follicles cultured within collagen gel: Reexpression of specific functions. *Biol Cell* 51, 315-325. doi:10.1111/j.1768-322X.1984.tb00310.x
- Coecke, S., Balls, M., Bowe, G. et al. (2005). Guidance on good cell culture practice – A report of the second ECVAM task force on good cell culture practice. *Altern Lab Anim* 33, 261-287. doi:10.1177/026119290503300313
- Cox, C. R., Lynch, S., Goldring, C. et al. (2020). Current perspective: 3D spheroid models utilizing human-based cells for investigating metabolism-dependent drug-induced liver injury. *Front Med Technol* 2, 611913. doi:10.3389/fmedt.2020.611913
- Crivellente, F., Hart, A., Hernandez-Jerez, A. F. et al. (2019). Establishment of cumulative assessment groups of pesticides for their effects on the thyroid. *EFSA J* 17, e05801. doi:10.2903/j.efs.2019.5801
- Curran, P. G. and DeGroot, L. J. (1991). The effect of hepatic enzyme-inducing drugs on thyroid hormones and the thyroid gland. *Endocr Rev* 12, 135-150. doi:10.1210/edrv-12-2-135
- Darnell, M., Ulvestad, M., Ellis, E. et al. (2012). In vitro evaluation of major in vivo drug metabolic pathways using primary human hepatocytes and HepaRG cells in suspension and a dynamic three-dimensional bioreactor system. *J Pharmacol Exp Ther* 343, 134-144. doi:10.1124/jpet.112.195834
- Deisenroth, C., Soldatow, V. Y., Ford, J. et al. (2020). Development of an in vitro human thyroid microtissue model for chemical screening. *Toxicol Sci* 174, 63-78. doi:10.1093/toxsci/kfz238
- Desai, P. K., Tseng, H. and Souza, G. R. (2017). Assembly of hepatocyte spheroids using magnetic 3D cell culture for CYP450 inhibition/induction. *Int J Mol Sci* 18, 1085. doi:10.3390/ijms18051085
- DeVito, M., Biegel, L., Brouwer, A. et al. (1999). Screening methods for thyroid hormone disrupters. *Environ Health Perspect* 107, 407-415. doi:10.1289/ehp.99107407
- Domingues, R., Font, P., Sobrinho, L. et al. (2009). A novel variant in *Serpina7* gene in a family with thyroxine-binding globulin deficiency. *Endocrine* 36, 83-86. doi:10.1007/s12020-009-9202-2
- Dumont, J. E. (1971). The action of thyrotropin on thyroid metabolism. *Vitam Horm* 29, 287-412. doi:10.1016/S0083-6729(08)60051-5
- Elaut, G., Henkens, T., Papeleu, P. et al. (2006). Molecular mechanisms underlying the dedifferentiation process of isolated hepatocytes and their cultures. *Curr Drug Metab* 7, 629-660. doi:10.2174/138920006778017759
- EC – European Commission, Directorate-General for Environment (2017). Supporting the organisation of a workshop on thyroid disruption – Final report. *Publications Office*. doi:10.2779/921523
- ECHA and EFSA, Joint Research Centre et al. (2018). Guidance for the identification of endocrine disruptors in the context of Regulations (EU) No 528/2012 and (EC) No 1107/2009. *EFSA J* 16, 1-135. doi:10.2903/j.efs.2018.5311
- Felmler, D. J., Grün, D. and Baumert, T. F. (2018). Zooming in on liver zonation. *Hepatology* 67, 784-787. doi:10.1002/hep.29554
- Findlay, K. A. B., Kaptein, E., Visser, T. J. et al. (2000). Characterization of the uridine diphosphate-glucuronosyltransferase-catalyzing thyroid hormone glucuronidation in man. *J Clin Endocrinol Metabol* 85, 2879-2883. doi:10.1210/jc.85.8.2879
- Foster, J. R., Tinwell, H. and Melching-Kollmuss, S. (2021). A review of species differences in the control of, and response to, chemical-induced thyroid hormone perturbations leading to thyroid cancer. *Arch Toxicol* 95, 807-836. doi:10.1007/s00204-020-02961-6
- Friedman, K. P., Watt, E. D., Hornung, M. W. et al. (2016). Tiered high-throughput screening approach to identify thyroperoxidase inhibitors within the toxcast phase I and II chemical libraries. *Toxicol Sci* 151, 160-180. doi:10.1093/toxsci/kfw034
- Friesema, E. C. H., Ganguly, S., Abdalla, A. et al. (2003). Identification of monocarboxylate transporter 8 as a specific thyroid hormone transporter. *J Biol Chem* 278, 40128-40135. doi:10.1074/jbc.M300909200
- Friesema, E. C. H., Jansen, J., Milici, C. et al. (2005). Thyroid hormone transporters. *Vitam Horm* 70, 137-167. doi:10.1016/S0083-6729(05)70005-4
- Fukuchi, M., Shimabukuro, M., Shimajiri, Y. et al. (2002). Evidence for a deficient pancreatic  $\beta$ -cell response in a rat model of hyperthyroidism. *Life Sci* 71, 1059-1070. doi:10.1016/S0024-3205(02)01791-5
- Gamage, N., Barnett, A., Hempel, N. et al. (2006). Human sulfotransferases and their role in chemical metabolism. *Toxicol Sci* 90, 5-22. doi:10.1093/toxsci/kfj061
- Garbi, C., Tacchetti, C. and Wollman, S. H. (1986). Change of inverted thyroid follicle into a spheroid after embedding in a collagen gel. *Exp Cell Res* 163, 63-77. doi:10.1016/0014-4827(86)90558-6
- Gardas, A. (1991). Laboratory tests: Level of T3, T4, TSH and anti-thyroid gland autoantibodies in the Polish population [Article in Polish]. *Endokrynol Pol* 42, 353-358.
- Gaskell, H. J. (2016). Development of a Spheroid Model to Investigate Drug-Induced Liver Injury (Thesis). University of Liverpool, UK. [https://livrepository.liverpool.ac.uk/3004330/1/200648599\\_Aug2016.pdf](https://livrepository.liverpool.ac.uk/3004330/1/200648599_Aug2016.pdf)
- Hammond, G. L., Hill, L. A. and Round, P. W. (2019). Roles of plasma binding proteins in modulation of hormone action and metabolism. In I. Huhtaniemi and L. Martini (eds), *Encyclopedia of Endocrine Diseases* (51-60). 2<sup>nd</sup> edition. doi:10.1016/B978-0-12-801238-3.64186-7
- Goodman, H. M. (2009). Chapter 3 – Thyroid gland. In H. M. Goodman (ed.), *Goodman's Basic Medical Endocrinology* (43-59). 4<sup>th</sup> edition. Elsevier. doi:10.1016/B978-0-12-373975-9.00003-3
- Gunness, P., Mueller, D., Shevchenko, V. et al. (2013). 3D organotypic cultures of human HepaRG cells: A tool for in vitro toxicity studies. *Toxicol Sci* 133, 67-78. doi:10.1093/toxsci/kft021
- Hallgren, S. and Darnerud, P. O. (2002). Polybrominated diphenyl ethers (PBDEs), polychlorinated biphenyls (PCBs) and chlorinated paraffins (CPs) in rats – Testing interactions and mechanisms for thyroid hormone effects. *Toxicology* 177, 227-243. doi:10.1016/s0300-483x(02)00222-6
- Hendriks, D. F. G., Puigvert, L. F., Messner, S. et al. (2016). Hepatic 3D spheroid models for the detection and study of com-



- pounds with cholestatic liability. *Sci Rep* 6, 35434. doi:10.1038/srep35434
- Hoekstra, R., Nibourg, G. A. A., Van Der Hoeven, T. V. et al. (2013). Phase 1 and phase 2 drug metabolism and bile acid production of HepaRG cells in a bioartificial liver in absence of dimethyl sulfoxide. *Drug Metab Dispos* 41, 562-567. doi:10.1124/dmd.112.049098
- Hohtari, H., Pakarinen, A. and Kauppila, A. (1987). Serum concentrations of thyrotropin, thyroxine, triiodothyronine and thyroxine binding globulin in female endurance runners and joggers. *Acta Endocrinol* 114, 41-46. doi:10.1530/acta.0.1140041
- Hood, A., Allen, M. L., Liu, Y. P. et al. (2003). Induction of T4 UDP-GT activity, serum thyroid stimulating hormone, and thyroid follicular cell proliferation in mice treated with microsomal enzyme inducers. *Toxicol Appl Pharmacol* 188, 6-13. doi:10.1016/S0041-008X(02)00071-6
- Huaman, C., Caron, S., Briand, O. et al. (2012). The human hepatocyte cell lines IHH and HepaRG: Models to study glucose, lipid and lipoprotein metabolism. *Arch Physiol Biochem* 118, 102-111. doi:10.3109/13813455.2012.683442
- Ito, M., Toyoda, N., Nomura, E. et al. (2011). Type 1 and type 2 iodothyronine deiodinases in the thyroid gland of patients with 3,5,3'-triiodothyronine-predominant Graves' disease. *Eur J Endocrinol* 164, 95-100. doi:10.1530/EJE-10-0736
- Janssen, S. T. and Janssen, O. E. (2017). Directional thyroid hormone distribution via the blood stream to target sites. *Mol Cell Endocrinol* 458, 16-21. doi:10.1016/j.mce.2017.02.037
- Jomaa, B., De Haan, L. H. J., Peijnenburg, A. A. C. M. et al. (2015). Simple and rapid in vitro assay for detecting human thyroid peroxidase disruption. *ALTEX* 32, 191-200. doi:10.14573/altex.1412201
- Jungsuwadee, P. and Vore, M. E. (2010). 4.26 – Efflux transporters. In C. A. McQueen (ed.), *Comprehensive Toxicology* (557-601). 2<sup>nd</sup> edition. Elsevier. doi:10.1016/B978-0-08-046884-6.00426-7
- Kammerer, S. and Küpper, J.-H. (2018). Human hepatocyte systems for in vitro toxicology analysis. *J Cell Biotechnol* 3, 85-93. doi:10.3233/jcb-179012
- Kanebratt, K. P., Janefeldt, A., Vilén, L. et al. (2021). Primary human hepatocyte spheroid model as a 3D in vitro platform for metabolism studies. *J Pharm Sci* 110, 422-431. doi:10.1016/j.xphs.2020.10.043
- Karwelat, D., Kühnlenz, J., Steger-Hartmann, T. et al. (2022). A rodent thyroid-liver chip to capture thyroid toxicity on organ functional level. *ALTEX*, online ahead of print. doi:10.14573/altex.2108262
- Kato, Y., Ikushiro, S. I., Emi, Y. et al. (2008). Hepatic UDP-glucuronosyltransferases responsible for glucuronidation of thyroxine in humans. *Drug Metab Dispos* 36, 51-55. doi:10.1124/dmd.107.018184
- Kester, M. H. A., van Dijk, C. H., Tibboel, D. et al. (1999). Sulfation of thyroid hormone by estrogen sulfotransferase. *J Clin Endocrinol Metab* 84, 2577-2580. doi:10.1210/jcem.84.7.5975
- Kraiem, Z., Sadeh, O. and Yosef, M. (1991). Iodide uptake and organification, tri-iodothyronine secretion, cyclic AMP accumulation and cell proliferation in an optimized system of human thyroid follicles cultured in collagen gel suspended in serum-free medium. *J Endocrinol* 131, 499-506. doi:10.1677/joe.0.1310499
- Kühnl, J., Tao, T. P., Brandmair, K. et al. (2021). Characterization of application scenario-dependent pharmacokinetics and pharmacodynamic properties of permethrin and hyperforin in a dynamic skin and liver multi-organ-chip model. *Toxicology* 448, 152637. doi:10.1016/j.tox.2020.152637
- Kusunoki, T., Nishida, S., Koezuka, M. et al. (2001). Morphological and functional differentiation of human thyroid cells in collagen gel culture. *Auris Nasus Larynx* 28, 333-338. doi:10.1016/S0385-8146(01)00109-2
- Langan, L. M., Dodd, N. J. F., Owen, S. F. et al. (2016). Direct measurements of oxygen gradients in spheroid culture system using electron parametric resonance oximetry. *PLoS One* 11, e0149492. doi:10.1371/journal.pone.0149492
- Lauschke, V. M., Hendriks, D. F. G., Bell, C. C. et al. (2016). Novel 3D culture systems for studies of human liver function and assessments of the hepatotoxicity of drugs and drug candidates. *Chem Res Toxicol* 29, 1936-1955. doi:10.1021/acs.chemrestox.6b00150
- Leemans, M., Couderq, S., Demeneix, B. et al. (2019). Pesticides with potential thyroid hormone-disrupting effects: A review of recent data. *Front Endocrinol* 10, 743. doi:10.3389/fendo.2019.00743
- Leite, S. B., Wilk-Zasadna, I., Zaldivar, J. M. et al. (2012). Three-dimensional HepaRG model as an attractive tool for toxicity testing. *Toxicol Sci* 130, 106-116. doi:10.1093/toxsci/kfs232
- Li, J., Settivari, R. S., Lebaron, M. J. et al. (2019). Functional comparison of HepaRG Cells and primary human hepatocytes in sandwich and spheroid culture as repeated-exposure models for hepatotoxicity. *Appl In Vitro Toxicol* 5, 187-195. doi:10.1089/aivt.2019.0008
- Lübberstedt, M., Müller-Vieira, U., Mayer, M. et al. (2011). HepaRG human hepatic cell line utility as a surrogate for primary human hepatocytes in drug metabolism assessment in vitro. *J Pharmacol Toxicol Methods* 63, 59-68. doi:10.1016/j.vascn.2010.04.013
- Mandon, M., Huet, S., Dubreil, E. et al. (2019). Three-dimensional HepaRG spheroids as a liver model to study human genotoxicity in vitro with the single cell gel electrophoresis assay. *Sci Rep* 9, 10548. doi:10.1038/s41598-019-47114-7
- Marchesini, G. R., Meimaridou, A., Haasnoot, W. et al. (2008). Biosensor discovery of thyroxine transport disrupting chemicals. *Toxicol Appl Pharmacol* 232, 150-160. doi:10.1016/j.taap.2008.06.014
- Marx, U., Akabane, T., Andersson, T. B. et al. (2020). Biology-inspired microphysiological systems to advance patient benefit and animal welfare in drug development. *ALTEX* 37, 364-394. doi:10.14573/altex.2001241
- Massart, C., Hody, B., Condé, D. et al. (1988). Functional properties of human thyroid follicles cultured within collagen gel. *Mol Cell Endocrinol* 56, 227-234. doi:10.1016/0303-7207(88)90065-2
- Mauchamp, J., Mirrione, A., Alquier, C. et al. (1998). Follicle-like structure and polarized monolayer: Role of the extracellular ma-

- trix on thyroid cell organization in primary culture. *Biol Cell* 90, 369-380. doi:10.1016/S0248-4900(98)80086-5
- Meek, M. E., Bucher, J. R., Cohen, S. M. et al. (2003). A framework for human relevance analysis of information on carcinogenic modes of action. *Crit Rev Toxicol* 33, 591-653. doi:10.1080/713608373
- Miyawaki, I., Tamura, A., Matsumoto, I. et al. (2012). The effects of clobazam treatment in rats on the expression of genes and proteins encoding glucuronosyltransferase 1A/2B (UGT1A/2B) and multidrug resistance-associated protein-2 (MRP2), and development of thyroid follicular cell hypertrophy. *Toxicol Appl Pharmacol* 265, 351-359. doi:10.1016/j.taap.2012.09.003
- Mondal, S., Raja, K., Schweizer, U. et al. (2016). Chemistry and biology in the biosynthesis and action of thyroid hormones. *Angew Chem Int Ed Engl* 55, 7606-7630. doi:10.1002/anie.201601116
- Murakami, M., Araki, O., Hosoi, Y. et al. (2001). Expression and regulation of type II iodothyronine deiodinase in human thyroid gland. *Endocrinology* 142, 2961-2967. doi:10.1210/endo.142.7.8280
- Murk, A. T. J., Rijntjes, E., Blaauboer, B. J. et al. (2013). Mechanism-based testing strategy using in vitro approaches for identification of thyroid hormone disrupting chemicals. *Toxicol In Vitro* 27, 1320-1346. doi:10.1016/j.tiv.2013.02.012
- Nagasaka, A. and Hidaka, H. (1976). Effect of antithyroid agents 6-propyl-2-thiouracil and 1-methyl-2-mercaptoimidazole on human thyroid iodide peroxidase. *J Clin Endocrinol Metab* 43, 152-158. doi:10.1210/jcem-43-1-152
- Nikiforov, Y. E., Biddinger, P. W. and Thompson L. D. R. (2018). *Diagnostic Pathology and Molecular Genetics of the Thyroid: A Comprehensive Guide for Practicing Thyroid Pathology*. 3rd edition. Lippincott Williams & Wilkins.
- Nikrodhanond, A. A., Ortiga-Carvalho, T. M., Shibusawa, N. et al. (2006). Dominant role of thyrotropin-releasing hormone in the hypothalamic- pituitary-thyroid axis. *J Biol Chem* 281, 5000-5007. doi:10.1074/jbc.M511530200
- Nishida, S., Hosokawa, K., Kusunoki, T. et al. (1993). Morphological properties of human thyroid tumor cells in collagen gel culture and metastatic or invasive ability. *Histol Histopathol* 8, 329-337.
- Noyes, P. D., Friedman, K. P., Browne, P. et al. (2019). Evaluating chemicals for thyroid disruption: Opportunities and challenges with in vitro testing and adverse outcome pathway approaches. *Environ Health Perspect* 127, 95001. doi:10.1289/EHP5297
- Ohnhaus, E. and Studer, H. (1983). A link between liver microsomal enzyme activity and thyroid hormone metabolism in man. *Br J Clin Pharmacol* 15, 71-76. doi:10.1111/j.1365-2125.1983.tb01466.x
- Ohtsuki, S., Schaefer, O., Kawakami, H. et al. (2012). Simultaneous absolute protein quantification of transporters, cytochromes P450, and UDP-glucuronosyltransferases as a novel approach for the characterization of individual human liver: Comparison with mRNA levels and activities. *Drug Metab Dispos* 40, 83-92. doi:10.1124/dmd.111.042259
- Okamura, Y., Shigemasa, C. and Tatsuhara, T. (1986). Pharmacokinetics of methimazole in normal subjects and hyperthyroid patients. *Endocrinol Jpn* 33, 605-615. doi:10.1507/endocrj1954.33.605
- Ollis, C. A., Fowles, A., Brown, B. L. et al. (1985). Human thyroid cells in monolayer retain the ability to secrete tri-iodothyronine in response to thyrotrophin. *J Endocrinol* 104, 285-290. doi:10.1677/joe.0.1040285
- Patel, J., Landers, K., Li, H. et al. (2011). Thyroid hormones and fetal neurological development. *J Endocrinol* 209, 1-8. doi:10.1530/JOE-10-0444
- Pilo, A., Ferdeghini, M., Iervasi, G. et al. (1990). Thyroidal and peripheral production of 3,5,3'-triiodothyronine in human by multicompartmental analysis. *Am J Physiol* 258, E715-126. doi:10.1152/ajpendo.1990.258.4.E715
- Ramaiahgari, S. C., Waidyanatha, S., Dixon, D. et al. (2017). Three-dimensional (3D) HepaRG spheroid model with physiologically relevant xenobiotic metabolism competence and hepatocyte functionality for liver toxicity screening. *Toxicol Sci* 159, 124-136. doi:10.1093/toxsci/kfx122
- Richardson, V. M., Ferguson, S. S., Sey, Y. M. et al. (2014). In vitro metabolism of thyroxine by rat and human hepatocytes. *Xenobiotica* 44, 391-403. doi:10.3109/00498254.2013.847990
- Richter, L. H. J., Kaminski, Y. R., Noor, F. et al. (2016). Metabolic fate of desomorphine elucidated using rat urine, pooled human liver preparations, and human hepatocyte cultures as well as its detectability using standard urine screening approaches. *Anal Bioanal Chem* 408, 6283-6294. doi:10.1007/s00216-016-9740-4
- Rouquié, D., Tinwell, H., Blanck, O. et al. (2014). Thyroid tumor formation in the male mouse induced by fluopyram is mediated by activation of hepatic CAR/PXR nuclear receptors. *Regul Toxicol Pharmacol* 70, 673-680. doi:10.1016/j.yrtph.2014.10.003
- Saito, Y., Onishi, N., Takami, H. et al. (2018). Development of a functional thyroid model based on an organoid culture system. *Biochem Biophys Res Commun* 497, 783-789. doi:10.1016/j.bbrc.2018.02.154
- Sasaki, M., Sawada, N., Minase, T. et al. (1991). Collagen-gel-embedded three-dimensional culture of human thyroid epithelial cells: Comparison between the floating sandwich method and the dispersed embedding method. *Cell Struct Funct* 16, 209-215. doi:10.1247/csf.16.209
- Schimek, K., Frentzel, S., Luettich, K. et al. (2020). Human multi-organ chip co-culture of bronchial lung culture and liver spheroids for substance exposure studies. *Sci Rep* 10, 7865. doi:10.1038/s41598-020-64219-6
- Sinha, R. A., Singh, B. K., Yen, P. M. et al. (2018). Direct effects of thyroid hormones on hepatic lipid metabolism. *Nat Rev Endocrinol* 14, 259-269. doi:10.1038/nrendo.2018.10
- Spinel-Gomez, C., Colin, I., van den Hove, M. F. et al. (1990). Correlated morphological and functional study of isolated rat thyroid follicles in suspension culture. *Mol Cell Endocrinol* 71, 141-153. doi:10.1016/0303-7207(90)90251-3
- Tascher, G., Burban, A., Camus, S. et al. (2019). In-depth proteome analysis highlights HepaRG Cells as a versatile cell system surrogate for primary human hepatocytes. *Cells* 8, 192. doi:10.3390/cells8020192



- Tinwell, H., Rouquié, D., Schorsch, F. et al. (2014). Liver tumor formation in female rat induced by fluopyram is mediated by CAR/PXR nuclear receptor activation. *Regul Toxicol Pharmacol* 70, 648-658. doi:10.1016/j.yrtph.2014.09.011
- Toda, S., Yonemitsu, N., Hikichi, Y. et al. (1992). Differentiation of human thyroid follicle cells from normal subjects and Basedow's disease in three-dimensional collagen gel culture. *Pathol Res Pract* 188, 874-882. doi:10.1016/S0344-0338(11)80247-5
- Toda, S., Aoki, S., Uchihashi, K. et al. (2011). Culture models for studying thyroid biology and disorders. *ISRN Endocrinol* 2011, 275782. doi:10.5402/2011/275782
- Tomida, T., Okamura, H., Satsukawa, M. et al. (2015). Multiparametric assay using HepaRG cells for predicting drug-induced liver injury. *Toxicol Lett* 236, 16-24. doi:10.1016/j.toxlet.2015.04.014
- Uhlén, M., Fagerberg, L., Hallström, B. M. et al. (2015). Proteomics. Tissue-based map of the human proteome. *Science* 347, 1260419. doi:10.1126/science.1260419
- Underhill, G. H. and Khetani, S. R. (2018). Bioengineered liver models for drug testing and cell differentiation studies. *Cell Mol Gastroenterol Hepatol* 5, 426-439.e1. doi:10.1016/j.jcmgh.2017.11.012
- Van der Spek, A. H., Fliers, E. and Boelen, A. (2017). The classic pathways of thyroid hormone metabolism. *Mol Cell Endocrinol* 458, 29-38. doi:10.1016/j.mce.2017.01.025
- Vargas-Uricoechea, H., Bonelo-Perdomo, A. and Sierra-Torres, C. H. (2014). Effects of thyroid hormones on the heart. *Clin Investig Arterioscler* 26, 296-309. doi:10.1016/j.arteri.2014.07.003
- Vickers, A. E. M., Heale, J., Sinclair, J. R. et al. (2012). Thyroid organotypic rat and human cultures used to investigate drug effects on thyroid function, hormone synthesis and release pathways. *Toxicol Appl Pharmacol* 260, 81-88. doi:10.1016/j.taap.2012.01.029
- Visser, W. E., Friesema, E. C. H. and Visser, T. J. (2011). Minireview: Thyroid hormone transporters: The knowns and the unknowns. *Mol Endocrinol* 25, 1-14. doi:10.1210/me.2010-0095
- Wang, J., Hallinger, D. R., Murr, A. S. et al. (2019). High-throughput screening and chemotype-enrichment analysis of ToxCast phase II chemicals evaluated for human sodium-iodide symporter (NIS) inhibition. *Environ Int* 126, 377-386. doi:10.1016/j.envint.2019.02.024
- Wang, Z.-Y., Li, W.-J., Li, Q.-G. et al. (2019). A DMSO-free hepatocyte maturation medium accelerates hepatic differentiation of HepaRG cells in vitro. *Biomed Pharmacother* 116, 109010. doi:10.1016/j.biopha.2019.109010
- Willoughby, K. A., McAndrews, M. P. and Rovet, J. (2013). Effects of early thyroid hormone deficiency on children's autobiographical memory performance. *J Int Neuropsychol Soc* 19, 419-429. doi:10.1017/S1355617712001488
- Xie, W., Barwick, J. L., Downes, M. et al. (2000). Humanized xenobiotic response in mice expressing nuclear receptor SXR. *Nature* 406, 435-439. doi:10.1038/35019116
- Yokoyama, Y., Sasaki, Y., Terasaki, N. et al. (2018). Comparison of drug metabolism and its related hepatotoxic effects in HepaRG, cryopreserved human hepatocytes, and HepG2 cell cultures. *Biol Pharm Bull* 41, 722-732. doi:10.1248/bpb.b17-00913
- Zellmer, S., Schmidt-Heck, W., Godoy, P. et al. (2010). Transcription factors ETF, E2F, and SP-1 are involved in cytokine-independent proliferation of murine hepatocytes. *Hepatology* 52, 2127-2136. doi:10.1002/hep.23930

#### Conflict of interest

Uwe Marx is shareholder and CSO of TissUse GmbH, which commercializes MPS platforms.

#### Data availability

The research data that are not included in the article are available upon request from the corresponding author.

#### Acknowledgements

This work was funded by Bayer AG through a Life Science Collaboration programme. We thank Detlef Stöckigt and Oliver Born for the development of the thyroid hormone-related LC-MS/MS analytical methods as well as Ilka Maschmeyer for her expertise during the initiation of the project.